

# Some perspective of thermodynamical and optical properties of black holes in Maxwell-dilaton-dRGT-like massive gravity

B. Eslam Panah<sup>1\*</sup>, N. Heidari<sup>1†</sup>, and M. Soleimani<sup>1</sup>

<sup>1</sup> *Department of Theoretical Physics, Faculty of Basic Sciences, University of Mazandaran, P. O. Box 47416-95447, Babolsar, Iran*

Motivated by integrating the dilaton field (as a UV correction) with dRGT-like massive gravity (as an IR correction) into Einstein gravity, we investigate the thermodynamic and optical properties of black holes within this gravitational framework. We begin by reviewing the black hole solutions in Maxwell-dilaton-dRGT-like massive gravity, followed by an analysis of how various parameters influence on the asymptotical behavior of the spacetime and the event horizon of these black holes. In the subsequent section, we examine the conserved and thermodynamic quantities associated with these black holes, paying particular attention to the effects of parameters like  $\beta$ ,  $\alpha$ , and the massive parameters ( $\eta_1$  and  $\eta_2$ ) on their local stability by simultaneously evaluating the heat capacity and temperature. We also adopt an alternative method to study phase transitions using geometrothermodynamics. Furthermore, we explore how the parameters of Maxwell-dilaton-dRGT-like massive gravity impacts the optical characteristics and radiative behavior of black holes. In particular, we analyze the effects of the dilaton coupling constant ( $\alpha$ ), charge ( $q$ ), the massive gravity parameter ( $\eta_1$ ), and the graviton mass ( $m_g$ ) on the radius of the photon sphere and the resulting black hole shadow. Moreover, the theoretical shadow radius is compared to the observational data from *SgrA\**. Additionally, we investigate the energy emission rate of these black holes, revealing that these parameters substantially influence the emission peak.

## I. INTRODUCTION

Based on observational data such as supernovae [1, 2] and cosmic microwave background (CMB) radiation [3, 4], our universe is undergoing an accelerating expansion. General relativity (GR) cannot describe this acceleration, which motivates the study of alternative theories of gravity. Massive gravity is one of the interesting alternative theories of gravity, which can explain the late-time acceleration without considering dark energy [5–9]. It is notable that in massive gravity, the graviton includes a mass ( $m_g$ ), which reduces to GR when  $m_g \rightarrow 0$ . Furthermore, the gravitational field can be understood as a theory of a spin–2 graviton in modern particle physics [10, 11]. Historically, Fierz and Pauli introduced the first version of massive gravity in 1939. This theory was a linear theory of massive gravity [12]. However, this linear theory of massive gravity has a fundamental flaw. Specifically, the Fierz-Pauli (FP) massive gravity does not account for the observational evidence from the solar system when  $m_g = 0$ . To address this issue, Vainshtein extended the FP theory to include a nonlinear framework [13]. Subsequently, Boulware and Deser discovered the presence of a ghost in this nonlinear theory, now known as the Boulware-Deser (BD) ghost [14]. In response to this challenge, several attempts have been made to eliminate the ghost, including the development of new massive gravity in three-dimensional spacetime [15]. In recent years, a ghost-free massive theory was introduced by de Rham-Gabadadze-Tolley, which is known as dRGT-massive gravity [16, 17]. Furthermore, dRGT-massive gravity removes the BD ghost in arbitrary dimensions of spacetime [18, 19].

Black holes provide intriguing opportunities to test the theoretical and phenomenological aspects of modified theories of gravity, such as dRGT-massive gravity. Research on black holes in the context of dRGT-massive gravity has been conducted in Refs. [20–35]. Considering black holes in massive gravity, it has been indicated that the final stage of Hawking evaporation could lead to the formation of a black hole remnant, potentially resolving the information paradox [32]. On the other hand, the presence of additional terms in black hole solutions may provide explanations for dark matter and dark energy within the framework of massive gravity. Additionally, it has been established that the massive graviton can serve as a substitute for the cosmological constant over cosmic distances [36–39].

A noteworthy study suggests that using a dynamic reference metric, rather than a static one, allows for the neglect of the BD-ghost in a nonlinear bimetric theory involving a massless spin–2 field [40]. In a different approach, Vegh introduced an alternative branch of dRGT-massive gravity by applying holographic principles and utilizing a singular reference metric [41]. This framework is recognized as a ghost-free theory of massive gravity. Building on Vegh’s work, numerous studies have examined various aspects of this theory, including black hole solutions and their thermodynamic properties, as detailed in Refs. [42–56]. An interesting study [57] discusses that the mass of a graviton ( $m_g$ ) is typically

---

\* email address: eslampanah@umz.ac.ir

† email address: heidari.n@gmail.com

very small in weak gravitational environments but can be significantly larger in strong gravity regimes, such as near black holes and other compact objects. Recent observations from the advanced LIGO/Virgo collaborations suggest there may be a tight constraint on the graviton mass [58, 59]. Additionally, various empirical and theoretical limits on the graviton's mass have been established [60–63]. From an astrophysical perspective, the properties of compact objects in the context of Vegh massive gravity have been explored in the literature, indicating that these compact objects (such as massive neutron and quark stars, white dwarfs, and dark energy stars) could be potential candidates for regions of mass gap [64–70]. Notably, a correspondence has been identified between the black hole solutions in conformal gravity and Vegh massive gravity theory [71]. It was found that Vegh's massive gravity can exhibit new phase transitions for topological black holes due to the presence of the graviton mass [72]. These issues prompted us to investigate this type of massive gravity (known as dRGT-like massive gravity) to explore some thermodynamic and optical properties of black holes.

The emergence of a scalar field in the low-energy limit of string theory has led many researchers to explore dilaton gravity from various perspectives. The interaction between the dilaton and other gauge fields significantly affects the resulting solutions [73–78]. Notably, it has been shown that the dilaton field can alter the asymptotic behavior of spacetime. Specifically, in the presence of one or two Liouville-type dilaton potentials, black hole spacetimes are found to be neither asymptotically flat nor (anti)-de Sitter ((A)dS) [79–86]. This occurs because the dilaton field does not approach zero as  $r \rightarrow \infty$ . Additionally, integrating three Liouville-type dilaton potentials allows for the construction of dilatonic black hole solutions within the (A)dS spacetime framework [87–90]. Research has also examined neutron stars in the context of dilaton gravity [91, 92], as well as combining dilaton gravity with other modified theories to derive black holes [93–102].

Combining a scalar field, such as the dilaton field, with the massive theory of gravity known as dilaton-massive gravity poses challenges due to the complexity of the field equations. It is notable that although dRGT massive gravity can explain the accelerated expansion of the Universe without dark energy, it is only valid for an open Friedman-Lemaître-Robertson-Walker (FLRW) solution and lacks stable solutions for a homogeneous and isotropic Universe [103]. Additionally, the scalar and vector perturbations in this massive theory of gravity face issues due to a strong coupling problem and a nonlinear ghost instability [104]. To address these challenges, considering additional degrees of freedom, such as an extra scalar field, has proven to be a fruitful approach. For example, the quasi-dilaton massive theory of gravity successfully explains the accelerated expansion of the Universe in FLRW cosmology [105]. However, this theory also encounters perturbation instability, leading to the development of various extensions [106–108], see Refs. [109–114], for more details about the importance of the study of quasi-dilaton massive gravity in cosmology. In this regard, a recent study has successfully extracted a black hole solution within dilaton-dRGT-like massive gravity [115]. Notably, dilaton-dRGT-like massive gravity arises from the coupling of the dilaton field to the terms involving the dRGT-like massive graviton. Generalizing to include the Maxwell field results in charged black holes within the framework of dilaton-dRGT-like massive gravity, or equivalently, black holes in Maxwell-dilaton-dRGT-like massive gravity [116]. Building on these recent advancements, our goal is to further explore and reveal additional properties of charged black hole solutions in dilaton-dRGT-like massive gravity.

## II. BLACK HOLE SOLUTIONS

The action of Maxwell-dilaton-dRGT-like massive gravity is given by [115, 116]

$$\mathcal{I} = \frac{1}{16\pi} \int_{\partial\mathcal{M}} d^4x \sqrt{-g} \left[ \mathcal{R} - F_{\mu\nu} F^{\mu\nu} - 2(\nabla\varphi)^2 - V(\varphi) + e^{-2\beta\varphi} m_g^2 \sum_i^4 \eta_i u_i(g, h) \right], \quad (1)$$

where  $\varphi(r)$  is the dilaton field, and  $V(\varphi)$  is a potential for  $\varphi(r)$ . Furthermore,  $F_{\mu\nu} = \partial_\mu A_\nu - \partial_\nu A_\mu$  is the electromagnetic tensor field, and  $A_\mu$  is the gauge potential. Notably, we set  $G = c = 1$  in the action (1), where  $c$  is the speed of light and  $G$  is the gravitational constant. Additionally,  $g$  refers to the determinant of the metric tensor  $g_{\mu\nu}$ , i.e.,  $g = \det(g_{\mu\nu})$ . Also,  $\mathcal{R}$  and  $m_g$  denote the Ricci scalar and the graviton mass, respectively. The exponential factor of the last term denotes the nonminimal coupling of the scalar dilaton field to the massive graviton with coupling constant  $\beta$ . The constants  $\eta_i$  serve as free parameters of the action. Indeed,  $\eta_i$ 's are arbitrary constants whose values can be determined according to observational or theoretical considerations. The quantities  $u_i$  are introduced as symmetric polynomials of the eigenvalues of the matrix  $K^\mu{}_\nu = \sqrt{g^{\mu\sigma} h_{\sigma\nu}}$ . Here,  $g_{\mu\nu}$  is the dynamical metric tensor, and  $h_{\mu\nu}$  is the reference metric.

In the action (1),  $u_i$  are given in the following form

$$u_i = \sum_{y=1}^i (-1)^{y+1} \frac{(i-1)!}{(i-y)!} u_{i-y} [K^y], \quad (2)$$

where  $u_{i-y} = 1$ , when  $i = y$ . In addition,  $[K] = K_a^a$  and  $[K^n] = (K^n)_a^a$ .

By varying the action with respect to the metric tensor  $g_{\mu\nu}$  and the gauge potential  $A_\mu$ , and the dilaton field  $\varphi$ , the equations of motion are given by [115, 116]

$$G_{\mu\nu} = 2\partial_\mu\varphi\partial_\nu\varphi - \frac{1}{2}(V(\varphi) + 2\partial^\sigma\varphi\partial_\sigma\varphi)g_{\mu\nu} + 2\left(F_{\mu\sigma}F^\sigma_\nu - \frac{1}{4}F^2g_{\mu\nu}\right) + e^{-2\beta\varphi}m_g^2\chi_{\mu\nu}, \quad (3)$$

$$\nabla^2\varphi = \frac{1}{4}\left(\frac{\partial V(\varphi)}{\partial\varphi} + 2\beta e^{-2\beta\varphi}m_g^2\sum_i^4\eta_i u_i(g, h)\right), \quad (4)$$

$$\nabla_\mu F^{\mu\nu} = 0, \quad (5)$$

where  $G_{\mu\nu}$  is the Einstein tensor.  $\chi_{\mu\nu}$  is referred to as the massive tensor in the following form

$$\chi_{\mu\nu} = -\sum_{i=1}^{d-2}\frac{\eta_i}{2}\left[u_i g_{\mu\nu} + \sum_{y=1}^i\frac{(-1)^y i!}{(i-y)!}u_{i-y}[K^y_{\mu\nu}]\right], \quad (6)$$

where  $d$  is related to the dimensions of spacetime. We work in a 4-dimensional spacetime, so  $d = 4$ .

We consider a 4-dimensional static spacetime with the following form

$$ds^2 = -f(r)dt^2 + \frac{dr^2}{f(r)} + r^2 R^2(r)(d\theta^2 + \sin^2\theta d\varphi^2), \quad (7)$$

where  $f(r)$  is the metric function.

Considering the spatial reference metric (or spatial fiducial metric) in the following form

$$h_{\mu\nu} = \text{diag}(0, 0, c_0^2, c_0^2 \sin^2\theta), \quad (8)$$

where  $c_0$  is a positive constant, the only non-zero components of  $u_i$  are  $u_1$  and  $u_2$ , and obtained as [115, 116]

$$\begin{aligned} u_1 &= \frac{2}{rR(r)}, \quad \& \quad u_2 = \frac{2}{r^2 R^2(r)}, \\ u_i &= 0, \quad \text{when } i > 2. \end{aligned} \quad (9)$$

Using  $A_\mu = (A_t, 0, 0, 0)$ , and Eqs. (5), and (7), the electromagnetic tensor field is given by  $F_{tr} = \frac{q}{r^2 R^2(r)}$ . Applying Eqs. (3), (4), and the 4-dimensional static spacetime (7), the metric function is obtained as [115, 116]

$$\begin{aligned} f(r) &= \frac{\gamma_{1,1}}{\gamma_{-1,1}}\left(\frac{b}{r}\right)^{\frac{-2\alpha^2}{\gamma_{1,1}}} - m_0 r^{\frac{\gamma_{1,-1}}{\gamma_{1,1}}} + \frac{\gamma_{1,1}^2}{\gamma_{1,-3}}\Lambda r^2\left(\frac{b}{r}\right)^{\frac{2\alpha^2}{\gamma_{1,1}}} \\ &\quad - \frac{\gamma_{1,1}^2 c_0 \eta_1 m_g^2 \left(\frac{b}{r}\right)^{\frac{-\xi_{1,2,0}}{\gamma_{1,1}}}}{\xi_{1,2,2}\xi_{2,2,-1}} - \frac{\gamma_{1,1}^2 c_0^2 \eta_2 m_g^2 \left(\frac{b}{r}\right)^{\frac{-\xi_{2,2,0}}{\gamma_{1,1}}}}{\xi_{1,1,-1}\xi_{1,2,-1}} \\ &\quad - \frac{2q^2 \gamma_{1,1}^2}{\gamma_{1,-1}\gamma_{1,-2}r^2}\left(\frac{b}{r}\right)^{\frac{-4\alpha^2}{\gamma_{1,1}}}, \end{aligned} \quad (10)$$

Also,  $\varphi(r)$ ,  $R(r)$  and  $V(\varphi)$  are extracted in the following forms [115, 116]

$$R(r) = e^{\alpha\varphi(r)}, \quad (11)$$

$$\varphi(r) = \frac{\alpha}{\gamma_{1,1}}\ln\left(\frac{b}{r}\right), \quad (12)$$

$$\begin{aligned} V(\varphi) &= 2\Lambda e^{2\alpha\varphi} + \frac{2\alpha^2 e^{\frac{2\varphi}{\alpha}}}{b^2 \gamma_{1,-1}} - \frac{2\alpha^2 q^2 e^{\frac{4\varphi}{\alpha}}}{b^4 \gamma_{1,-2}} \\ &\quad + \frac{4\xi_{1,1,0} c_0 \eta_1 m_g^2 e^{\frac{\varphi\xi_{0,-2,1}}{\alpha}}}{b\xi_{2,2,-1}} + \frac{2\xi_{1,1,0} c_0^2 \eta_2 m_g^2 e^{\frac{2\varphi\xi_{0,-1,1}}{\alpha}}}{b^2 \xi_{1,1,-1}}, \end{aligned} \quad (13)$$

where  $\gamma_{i,j} = i\alpha^2 + j$ , and  $\xi_{i,j,k} = i\alpha^2 + j\alpha\beta + k$ , where they are dimensionless quantities. In addition,  $\alpha$  and  $b$  are constants. The dimension of  $b$  is **Length**, i.e.,  $[b] = L$ , however  $\alpha$  is dimensionless parameter. Notably,  $\alpha$  is the parameter of the dilaton field.

Here, we are going to investigate the massive coefficients via dimensional analysis. In general, all terms of Eq. (10) must be dimensionless. On the other hand, in dimensional analysis we know that  $[m_g] = [r] = [b] = L$  and  $[\alpha] = [\gamma_{i,j}] = [\xi_{i,j,k}] = 1$ . Indeed,  $\alpha$ ,  $\gamma_{i,j}$ , and  $\xi_{i,j,k}$ , are dimensionless. Also, the dimension  $m_0$  is  $[m_0] = L^{\frac{\gamma_{-1,1}}{\gamma_{1,1}}}$ . Therefore, the dimensional interpretation of massive terms are

$$[\eta_1 c_0] = L^{-3}, \quad (14)$$

$$[\eta_2 c_0^2] = L^{-2}, \quad (15)$$

Using Eqs. (14), and (15), one can show that massive coefficients are, dimensionally,

$$[c_0] = L \quad \& \quad [\eta_i] = L^{-4}, \quad i = 1, 2 \quad (16)$$

Now, we can calculate the Ricci scalar by using the 4-dimensional spacetime in Eq. (7), and the metric function (10). After some complete calculations, we can obtain the Ricci scalar in the following form

$$\begin{aligned} R = & \frac{6\Lambda\gamma_{1,-2}}{\gamma_{1,-3}} \left(\frac{b}{r}\right)^{\frac{2\alpha^2}{\gamma_{1,1}}} - \frac{2m_0\alpha}{\gamma_{1,1}^2 r^{\frac{\gamma_{1,3}}{\gamma_{1,1}}}} \\ & + \frac{2\xi_{1,-1,1}\xi_{1,1,1}}{\gamma_{1,1}\gamma_{1,-1}r^2} \left(\frac{b}{r}\right)^{\frac{-2\alpha^2}{\gamma_{1,1}}} + \frac{4\alpha^2 q^2}{\gamma_{1,-1} \left(\frac{b}{r}\right)^{\frac{4\alpha^2}{\gamma_{1,1}}} r^4} \\ & + \frac{c_0\eta_1 m_g^2 \xi_{2,2,3}}{\xi_{2,2,-1} \left(\frac{b}{r}\right)^{\frac{\xi_{1,2,0}}{\gamma_{1,1}}} r} + \frac{2c_0^2 \eta_2 m_g^2 \xi_{1,1,1} \xi_{1,2,1}}{\xi_{1,2,-1} \xi_{1,1,-1} \left(\frac{b}{r}\right)^{\frac{\xi_{2,2,0}}{\gamma_{1,1}}} r^2}, \end{aligned} \quad (17)$$

where indicates that the Ricci scalar is not constant, and it depends on all of parameters of charged black holes in dillaton-dRGT-like massive gravity. Furthermore, the Ricci scalar diverge at  $r = 0$  (i.e.  $\lim_{r \rightarrow 0} R \rightarrow \infty$ ).

Using the spacetime (7), we obtain the Kretschmann scalar in the following form

$$\begin{aligned} R_{\alpha\beta\gamma\delta}R^{\alpha\beta\gamma\delta} = & \frac{8R'^2 f^2}{R^2} + \frac{8R'R''(4f + rf')f}{rR^2} + \frac{8R''Rff'}{rR^2} + f'^2 \\ & + \frac{4R^4 f^2}{R^4} + \frac{16R^3 f^2}{rR^3} + \frac{4f'^2}{r^2} + \frac{4(f-1)^2}{r^4} \\ & + \frac{4R^2}{r^2 R^4} [14R^2 f^2 + 4rR^2 ff' + r^2 R^2 f'^2 - 2f] \\ & + \frac{8R'}{r^3 R^3} [2R^2 f^2 + r^2 R^2 f'^2 + 2rR^2 ff' - 2f], \end{aligned} \quad (18)$$

where  $f = f(r)$ , and  $R = R(r)$ . By substituting the metric function (Eq. (10)) and Eq. (11) into the Kretschmann scalar (Eq. (18)), we find that the Kretschmann scalar diverges at  $r = 0$ . This indicates the presence of a curvature singularity at  $r = 0$ .

The investigation of the asymptotic behavior of the metric function is intriguing, as it may depend on all the parameters of the theory. Our analysis indicates that the parameters  $\alpha$  and  $\beta$  play an important role in determining the asymptotic behavior of spacetime. We categorize the effects of various parameters on the asymptotic behavior of spacetime into three parts by adjusting the values of  $\alpha$  and  $\beta$ , which are:

i) For all values of  $\alpha$ , the asymptotic behavior of the spacetime is determined solely by the following term:

$$\lim_{r \rightarrow \infty} f(r) \rightarrow \frac{\gamma_{1,1}^2}{\gamma_{1,-3}} \Lambda r^2 \left(\frac{b}{r}\right)^{\frac{2\alpha^2}{\gamma_{1,1}}}, \quad (19)$$

which shows the spacetime will not be asymptotically (A)dS, because it depends on both  $\Lambda$  and  $\alpha$ .

ii) Considering  $\beta > \frac{-\gamma_{2,-1}}{2\alpha}$ , the asymptotical behavior of the spacetime is given by

$$\lim_{r \rightarrow \infty} f(r) \longrightarrow \frac{\gamma_{1,1}^2}{\gamma_{1,-3}} \Lambda r^2 \left( \frac{b}{r} \right)^{\frac{2\alpha^2}{\gamma_{1,1}}} - \frac{\gamma_{1,1}^2 c_0 \eta_1 m_g^2 r \left( \frac{b}{r} \right)^{\frac{-\xi_{1,2,0}}{\gamma_{1,1}}}}{\xi_{1,2,2} \xi_{2,2,-1}}, \quad (20)$$

which reveals that the asymptotic behavior of the spacetime depends on the cosmological constant ( $\Lambda$ ), the parameters of the dilaton field ( $\alpha$ ), the parameter of the reference metric ( $c_0$ ), massive gravity ( $\eta_1$ ), and also the graviton mass ( $m_g$ ).

iii) For  $\alpha > -\beta$ , we find that

$$\lim_{r \rightarrow \infty} f(r) \longrightarrow \frac{\gamma_{1,1}^2}{\gamma_{1,-3}} \Lambda r^2 \left( \frac{b}{r} \right)^{\frac{2\alpha^2}{\gamma_{1,1}}} - \frac{\gamma_{1,1}^2 c_0 \eta_1 m_g^2 r \left( \frac{b}{r} \right)^{\frac{-\xi_{1,2,0}}{\gamma_{1,1}}}}{\xi_{1,2,2} \xi_{2,2,-1}} - \frac{\gamma_{1,1}^2 c_0^2 \eta_2 m_g^2 \left( \frac{b}{r} \right)^{\frac{-\xi_{2,2,0}}{\gamma_{1,1}}}}{\xi_{1,1,-1} \xi_{1,2,-1}}, \quad (21)$$

where it is clear that the asymptotic behavior of the spacetime is determined by all of the parameters of the system, such as  $\Lambda$ ,  $\alpha$ ,  $\beta$ ,  $c_0$ ,  $\eta_1$ ,  $\eta_2$ , and  $m_g$ .

To find the roots of the metric function  $f(r)$ , we need to solve the equation (10). Finding an exact solution is complicated, so we have plotted  $f(r)$  versus  $r$  in Fig. 1. Our analysis reveals that these black holes can have multiple horizons, depending on the values of various parameters. We summarize our findings regarding the effects of these parameters in four panels.

1- **Up-left panel in Fig. 1:** There exists a critical mass value ( $m_{critical}$ ) for these black holes, which corresponds to one event horizon and external root (indicated by the dashed line in this panel). When  $m_0 < m_{critical}$ , there are three real roots: one event horizon and two inner roots. However, when the mass exceeds the critical value (i.e.,  $m_0 > m_{critical}$ ), the number of roots decreases from two to one. Additionally, our findings highlight that as  $m_0$  increases, the event horizon of the black hole also expands. In other words, the radius of the massive black hole increases, as we anticipated.

2- **Up-right panel in Fig. 1:** Similar to the previous case, a critical value for the electrical charge ( $q_{critical}$ ) exists in which the black holes encounter one event horizon and one external root (see the dashed line in the up-right panel of Fig. 1). Also, for  $q < q_{critical}$ , there are three real roots (one event horizon and two inner roots). On the other hand, for  $q > q_{critical}$ , the number of roots decreases from two to one. In addition, by increasing  $q$ , the radius of the black hole increases.

3- **Down-left panel in Fig. 1:** There is a critical value for  $\alpha$ , in which the black holes have two roots (one event horizon and one external root), see dashed line in the down-left panel in Fig. 1. For  $\alpha > \alpha_{critical}$ , there are three real roots (one event horizon and two inner roots). For  $\alpha < \alpha_{critical}$ , the number of roots decreases from two to one root. In other words, black holes with large values of the dilaton field encounter multiple horizons. Furthermore, a large value of the dilaton field leads to large black holes.

4- **Down-right panel in Fig. 1:** We adjust the coupling constant  $\beta$  to examine its influence on the number of roots of the metric function. Our findings reveal that for  $\beta_{critical}$ , the black holes encounter one event horizon and one external root (see the dashed line in the down-right panel of Fig. 1). Also, for  $\beta > \beta_{criticality}$ , there are three roots. In contrast, for  $\beta < \beta_{criticality}$ , the black holes exhibit only one real root, corresponding to the event horizon. Additionally, a higher value of the coupling constant results in larger black holes.

### III. THERMODYNAMICS AND GEOMETROTHERMODYNAMICS

#### A. Thermodynamic Quantities

In this section, we will examine the conserved and thermodynamic quantities of charged black holes in dilaton-dRGT-like massive gravity. We will then assess how various parameters of these black holes influence thermal stability regions and phase transition points. This will be done using heat capacity and geometrothermodynamics approaches.

Applying the surface gravity ( $\kappa$ ), the Hawking temperature of such black holes are given by [116]

$$T = \frac{\kappa}{2\pi} = \frac{f'(r)|_{r=r_+}}{4\pi} = \frac{-\gamma_{1,1}}{4\pi\gamma_{1,-1}r_+} \left( \frac{b}{r_+} \right)^{\frac{-2\alpha^2}{\gamma_{1,1}}} - \frac{\gamma_{1,1}\Lambda r_+}{4\pi} \left( \frac{b}{r_+} \right)^{\frac{2\alpha^2}{\gamma_{1,1}}} - \frac{\gamma_{1,1}c_0\eta_1 m_g^2 \left( \frac{b}{r_+} \right)^{\frac{-\xi_{1,2,0}}{\gamma_{1,1}}}}{4\pi\xi_{2,2,-1}} - \frac{\gamma_{1,1}c_0^2\eta_2 m_g^2 \left( \frac{b}{r_+} \right)^{\frac{-\xi_{2,2,0}}{\gamma_{1,1}}}}{4\pi\xi_{1,1,-1}r_+} + \frac{q^2\gamma_{1,1}}{2\pi\gamma_{1,-2}r_+^3} \left( \frac{b}{r_+} \right)^{\frac{-4\alpha^2}{\gamma_{1,1}}}. \quad (22)$$

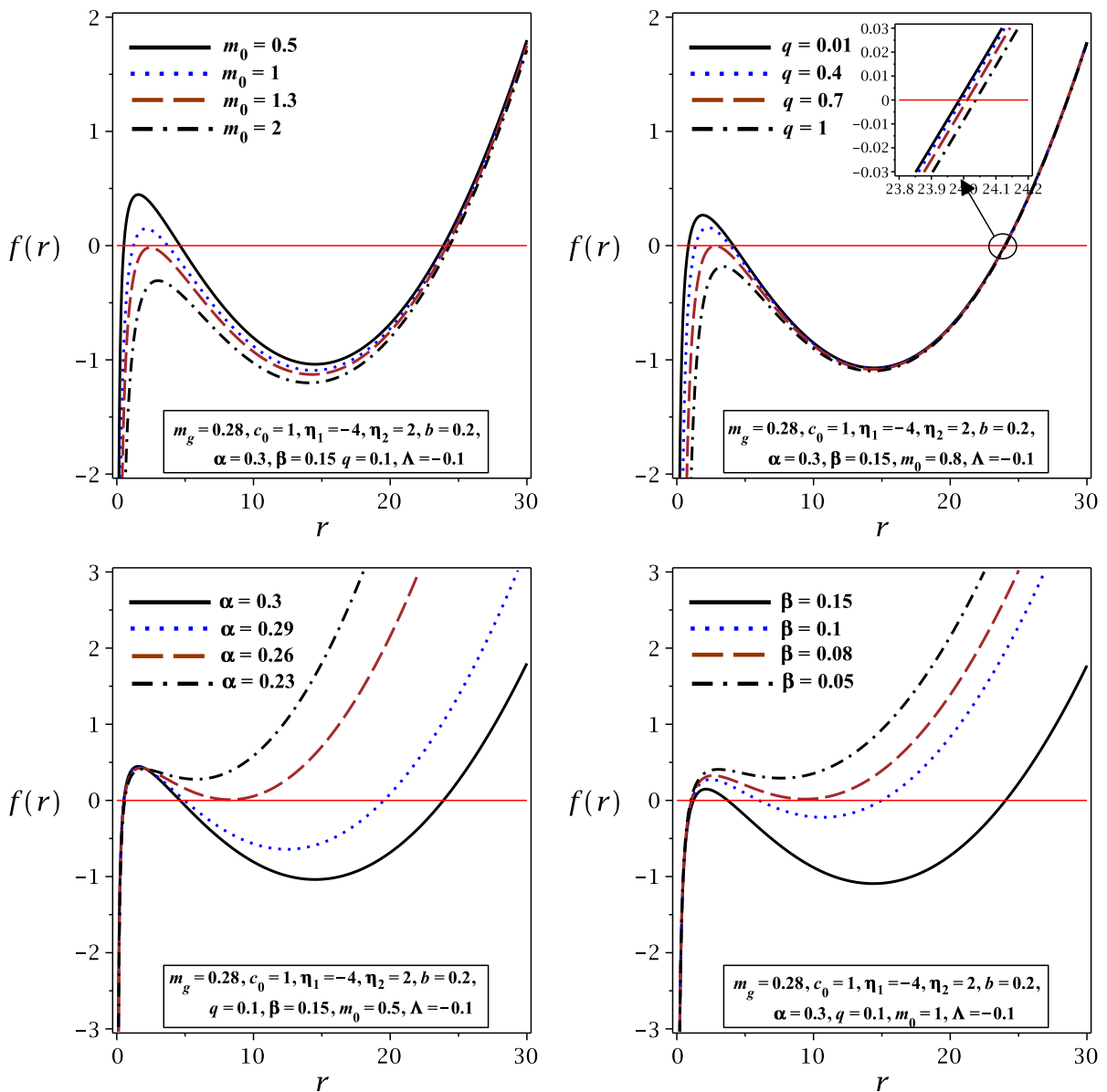


FIG. 1: The metric function  $f(r)$  versus  $r$  for different values of parameters.

The entropy of such black holes is obtained in the following form by using Wald's approach [116]

$$S = \pi r_+^2 \left( \frac{b}{r_+} \right)^{\frac{2\alpha^2}{\gamma_{1,1}}}, \quad (23)$$

where the entropy is altered by the presence of a dilaton field. Importantly, the modified entropy, as expressed in equation (23), simplifies to the standard form,  $S = \pi r_+^2$ , when the dilaton field is not present (i.e., when  $\alpha = 0$ ). In contrast, as  $\alpha$  approaches infinity, the modified entropy (Eq. (23)) converges to a constant value that depends on the coupling constant ( $b$ ). Specifically, we have  $\lim_{\alpha \rightarrow \infty} \left( \pi r_+^2 \left( \frac{b}{r_+} \right)^{\frac{2\alpha^2}{\alpha^2+1}} \right) = \pi b^2$ . This demonstrates one of the effects of the dilaton field on entropy.

Using the Ashtekar-Magnon-Das (AMD) approach, we can extract the total mass of these black holes as follows

[116]

$$M = \frac{-r_+}{2\gamma_{1,-1}} + \frac{\gamma_{1,1}\Lambda r_+^3}{2\gamma_{1,-3}} \left(\frac{b}{r_+}\right)^{\frac{4\alpha^2}{\gamma_{1,1}}} + \frac{q^2\gamma_{1,1}}{\gamma_{1,-1}\gamma_{1,-2}r_+} \left(\frac{b}{r_+}\right)^{\frac{-2\alpha^2}{\gamma_{1,1}}} - \frac{\gamma_{1,1}^2 c_0 \eta_1 m_g^2 r_+^2 \left(\frac{b}{r_+}\right)^{\frac{\xi_{1,-2,0}}{\gamma_{1,1}}}}{2\xi_{1,2,2}\xi_{2,2,-1}} - \frac{\gamma_{1,1} c_0^2 \eta_2 m_g^2 r_+ \left(\frac{b}{r_+}\right)^{\frac{\xi_{0,-2,0}}{\gamma_{1,1}}}}{2\xi_{1,1,-1}\xi_{1,2,1}}, \quad (24)$$

where it reduces to the total mass of black holes in dRGT-like massive gravity in the absence of the dilaton field ( $\alpha = 0$ ) as

$$\lim_{\alpha \rightarrow 0} M = \frac{r_+}{2} + \frac{c_0^2 \eta_2 m_g^2 r_+}{2} + \frac{c_0 \eta_1 m_g^2 r_+^2}{4} - \frac{\Lambda r_+^3}{6} + \frac{q^2}{2r_+}, \quad (25)$$

that it diverges at  $r_+ = 0$  due to the presence of electric charge. However, the total mass (Eq. (24)) of charged black holes in dilaton-dRGT-like massive gravity, in the absence of the cosmological constant and with a very large value for  $\alpha$ , takes the following form

$$\lim_{\alpha \rightarrow \infty} M = -\frac{c_0^2 \eta_2 m_g^2 b r_+}{2}, \quad (26)$$

where the results indicate that the electric charge disappears due to the influence of the strong dilaton field. However, the coupling between  $b$  (the coupling constant) and the parameters of massive gravity remains intact in an environment with a strong dilaton field. Additionally, equation (26) presents two noteworthy points

- i) The total mass is zero at  $r_+ = 0$  when the dilaton field is strong.
- ii) The signature of  $\eta_2$  must be negative to prevent the total mass from taking on a negative value.

The electric potential  $\Phi$  of the charge black holes in dilaton-dRGT-like massive gravity is determined as follows [116]

$$\Phi = \frac{2\gamma_{1,1}q}{\gamma_{1,-1}\gamma_{1,-2}r_+} \left(\frac{b}{r_+}\right)^{\frac{-2\alpha^2}{\gamma_{1,1}}}, \quad (27)$$

where it reduces to  $\Phi = \frac{q}{r_+}$  when  $\alpha = 0$ . Also, for  $\alpha \rightarrow \infty$ ,  $\Phi$  is zero (i.e,  $\lim_{\alpha \rightarrow \infty} \Phi = 0$ ). This indicate that the electric potential disappears when the effect of the dilaton field is very strong.

It is easy to demonstrate that the conserved quantities and thermodynamic variables comply with the first law of thermodynamics in the following form

$$dM = TdS + \Phi dq. \quad (28)$$

## B. Heat Capacity and Thermal Stability

Here, we analyze heat capacity and geometrothermodynamics to identify thermal stability and phase transition points simultaneously. Specifically, we will examine how various parameters of charged black holes in dilaton-massive gravity affects areas of thermal stability and points of phase transition by applying both heat capacity and geometrothermodynamics approaches.

The study of heat capacity provides crucial information about areas of thermal stability and points of phase transition within the context of the canonical ensemble. Specifically, a positive heat capacity indicates thermal stability, while a negative heat capacity suggests instability. Divergences in heat capacity correspond to phase transition points. Additionally, the roots of heat capacity determine the boundary points of thermal systems.

The heat capacity is defined as

$$C_Q = T \left( \frac{\partial S}{\partial T} \right)_Q = \frac{\left( \frac{\partial M(S,Q)}{\partial S} \right)_Q}{\left( \frac{\partial^2 M(S,Q)}{\partial S^2} \right)_Q} = \frac{M_S}{M_{SS}}, \quad (29)$$

where  $M_S = \left(\frac{\partial M(S,Q)}{\partial S}\right)_Q$ , and  $M_{SS} = \left(\frac{\partial^2 M(S,Q)}{\partial S^2}\right)_Q$ . So, we have to rewrite the mass as a function of the extensive quantities  $S$  and  $Q$  for obtaining the heat capacity (29). Using Eqs. (22), (23) and by replacing them in Eq. (24), the mass  $M(S, Q)$  is found as

$$M(S, Q) = \frac{-b}{2\gamma_{1,-1}} \left(\frac{S}{\pi b^2}\right)^{\frac{\gamma_{1,1}}{2}} + \frac{\gamma_{1,1}\Lambda b^3}{2\gamma_{1,-3}} \left(\frac{S}{\pi b^2}\right)^{\frac{\gamma_{-1,3}}{2}} + \frac{Q^2\gamma_{1,1}}{\gamma_{1,-1}\gamma_{1,-2}b} \left(\frac{S}{\pi b^2}\right)^{\frac{\gamma_{1,-1}}{2}} - \frac{\gamma_{1,1}^2 c_0 \eta_1 m_g^2 b^2 \left(\frac{S}{\pi b^2}\right)^{\frac{\xi_{1,2,2}}{2}}}{2\xi_{1,2,2}\xi_{2,2,-1}} - \frac{\gamma_{1,1} c_0^2 \eta_2 m_g^2 b \left(\frac{S}{\pi b^2}\right)^{\frac{\xi_{1,2,1}}{2}}}{2\xi_{1,1,-1}\xi_{1,2,1}}. \quad (30)$$

where  $q = Q$ .

By applying Eqs. (29) and (30), we can express the heat capacity in the following manner

$$C_Q = \frac{(\mathcal{A}_1 + \mathcal{A}_2 + \mathcal{A}_3 + \mathcal{A}_4) S}{\frac{-\gamma_{1,-1}\mathcal{A}_1}{2} + \frac{\mathcal{A}_2\xi_{1,2,0}}{2} - \frac{Q^2\gamma_{1,-3}\xi_{1,1,-1}\xi_{2,2,-1}\left(\frac{S}{\pi b^2}\right)^{\xi_{1,0,0}}}{\gamma_{1,-2}} + \mathcal{A}_5}, \quad (31)$$

where  $\mathcal{A}_1, \mathcal{A}_2, \mathcal{A}_3, \mathcal{A}_4$ , and  $\mathcal{A}_5$  are

$$\mathcal{A}_1 = \frac{\xi_{1,1,-1}\xi_{2,2,-1}\Lambda S^2}{\pi^2}, \quad (32)$$

$$\mathcal{A}_2 = c_0\eta_1 m_g^2 b^3 \gamma_{1,1}\xi_{1,1,-1} \left(\frac{S}{\pi b^2}\right)^{\frac{\xi_{2,2,3}}{2}}, \quad (33)$$

$$\mathcal{A}_3 = c_0^2\eta_2 m_g^2 b^2 \xi_{2,2,-1} \left(\frac{S}{\pi b^2}\right)^{\xi_{1,1,1}}, \quad (34)$$

$$\mathcal{A}_4 = \left(\frac{-2Q^2}{\gamma_{1,-2}\left(\frac{S}{\pi b^2}\right)^{\alpha^2}} - \frac{b^2\left(\frac{S}{\pi b^2}\right)^{\gamma_{1,1}}}{\gamma_{1,-1}}\right) \xi_{1,1,-1}\xi_{2,2,-1}, \quad (35)$$

$$\mathcal{A}_5 = \left[c_0^2\eta_2 m_g^2 \xi_{1,2,-1} \left(\frac{S}{\pi b^2}\right)^{\xi_{0,1,0}} + \xi_{1,1,-1}\right] b^2 \left(\frac{S}{\pi b^2}\right)^{\gamma_{1,1}}. \quad (36)$$

We focus on studying heat capacity and temperature to determine four key properties of black holes:

- i) Thermal stability is characterized by the condition  $C_Q > 0$ .
- ii) The point where the heat capacity  $C_Q = T = 0$  is recognized as a physical limitation point.
- iii) Positive and negative temperature values indicate physical and non-physical black holes, respectively.
- iv) The divergences in heat capacity are associated with the critical points of phase transitions in black holes.

Based on the reasons provided, we plot the Hawking temperature ( $T$ ) and heat capacity ( $C_Q$ ) against entropy ( $S$ ) in Figs. 2-5. This allows us to examine the effects of the parameters of charged black holes in dilaton-dRGT-like massive gravity on thermal stability and phase transition points.

Our analysis reveals two divergence points and one zero point for the heat capacity, which we denote as  $S_{div_1}$  and  $S_{div_2}$  for the first and second divergence points, respectively. Additionally, we identify the root of the heat capacity as  $S_0$ . We categorize the behavior of heat capacity into four distinct areas (see Figs. 2-5):

**First area ( $S_1$ ):** This area is defined as being between 0 and  $S_0$  (i.e.,  $0 \leq S < S_0$ ). We refer to these as very small black holes. These black holes are considered non-physical objects because they have a negative temperature, and their heat capacity is also negative.

**Second area ( $S_2$ ):** This area lies between  $S_0$  and the first divergence point of the heat capacity (i.e.,  $S_0 < S < S_{div_1}$ ). We refer to this area as small black holes. In this area, both the temperature and heat capacity of the small black holes are positive. Therefore, the small charged black holes in dilaton-dRGT-like massive gravity meets the criteria for thermal stability and physical conditions.

**Third area ( $S_3$ ):** This area lies between  $S_{div_1}$  and  $S_{div_2}$  (i.e.,  $S_{div_1} < S < S_{div_2}$ ). We refer to this area as medium black holes. While the temperature of a medium black hole is positive, its heat capacity is negative. As a result, these black holes are unstable because they do not meet the conditions for thermal stability.

**Fourth area ( $S_4$ ):** This area pertains to  $S > S_{div_2}$ , which we refer to as large black holes. In this region, both the temperature and heat capacity of the large black holes are positive, indicating that they can simultaneously satisfy thermal stability and physical conditions.

We study the effects of  $\alpha$ ,  $\beta$ ,  $\eta_1$ , and  $\eta_2$  on the temperature and heat capacity of charged black holes in dilaton-dRGT-like massive gravity in figures 2-5.

**I. The impact of  $\alpha$ :** We investigate the effect of  $\alpha$  on the thermal stability area shown in Fig. 2. Our findings indicate that increasing the value of  $\alpha$  causes the first divergence point ( $S_{div1}$ ) and the zero point of the heat capacity ( $S_0$ ) to shift toward larger and smaller entropies, respectively. This shift results in an expansion of the stable area  $S_2$  ( $S_0 < S < S_{div1}$ ). However, the stable area for large black holes (denoted as the fourth area or  $S_4$ ) decreases as  $\alpha$  increases because  $S_{div2}$  moves to larger entropy values. Since the change in  $S_4$  is greater than that in  $S_2$ , the overall thermal stability area decreases with an increase in  $\alpha$ .

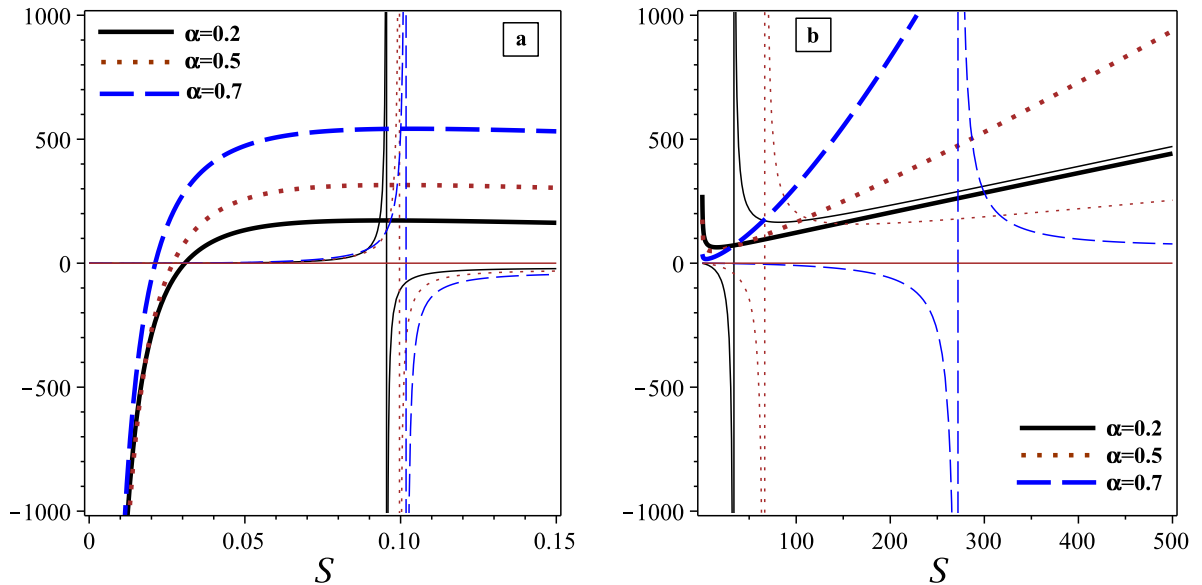


FIG. 2: The heat capacity ( $C_Q$ ) and the Hawking temperature ( $T$ ) versus entropy ( $S$ ) for different values of  $\alpha$  by considering  $Q = b = \beta = -\eta_2 = 0.1$ ,  $\eta_1 = 0.5$ ,  $\Lambda = -0.1$ ,  $c_0 = 1$ , and  $m_g = 0.2$ . Bold lines represent the Hawking temperature ( $T$ ), while thin lines indicate the heat capacity ( $C_Q$ )

**II. The impact of  $\beta$ :** We assess the impact of  $\beta$  on the thermal stability areas illustrated in Fig. 3. Our findings indicate that the thermal stability areas ( $S_2$  and  $S_4$ ) of charged black holes in dilaton-dRGT-like massive gravity expand as the value of  $\beta$  increases. Specifically, as  $\beta$  rises,  $S_{div1}$  shifts to higher entropy, while  $S_0$  remains unchanged. This results in an increased stable area for  $S_2$  (where  $S_0 < S < S_{div1}$ ). Additionally,  $S_{div2}$  moves towards lower entropy with increasing  $\beta$ , further enhancing the thermal stability area for larger black holes.

**III. The impact of  $\eta_1$ :** The impact of  $\eta_1$  on the thermal stability areas of charged black holes in dilaton-dRGT-like massive gravity is illustrated in Fig. 4. As  $\eta_1$  increases,  $S_{div1}$  shifts to higher entropy values, while  $S_0$  remains unchanged. This shift expands the thermal stability area within the range  $S_0 < S < S_{div1}$ . Furthermore, the second divergence point decreases as  $\eta_1$  increases, which further enhances the thermal stability area of  $S_2$ . Consequently, the thermal stability areas of charged black holes in dilaton-dRGT-like massive gravity expand when the value of  $\eta_1$  is large.

**IV. The impact of  $\eta_2$ :** We examine the impact of  $\eta_2$  on the thermal stability areas of charged black holes in dilaton-dRGT-like massive gravity, as illustrated in Fig. 5. Increasing  $\eta_2$  causes  $S_{div1}$  and  $S_{div2}$  to shift towards smaller and larger entropy values, respectively, while  $S_0$  remains unchanged. This results in a reduction of thermal stability regions in both the ranges  $S_0 < S < S_{div1}$  and  $S > S_{div2}$ . Consequently, the thermal stability areas of these black holes diminish as  $\eta_2$  increases.

By examining the heat capacity in Figs. 2-5, we identify two divergences in the heat capacity, denoted as  $S_{div1}$  and  $S_{div2}$ . Between these two divergence points, the black holes are physical and unstable, characterized by positive temperature and negative heat capacity. This leads to a phase transition from small entropy black holes to large entropy black holes. This phase transition is analogous to the van der Waals phase transition observed in fluids. Research has shown that the thermodynamics of an asymptotically AdS metric in four-dimensional spacetime closely

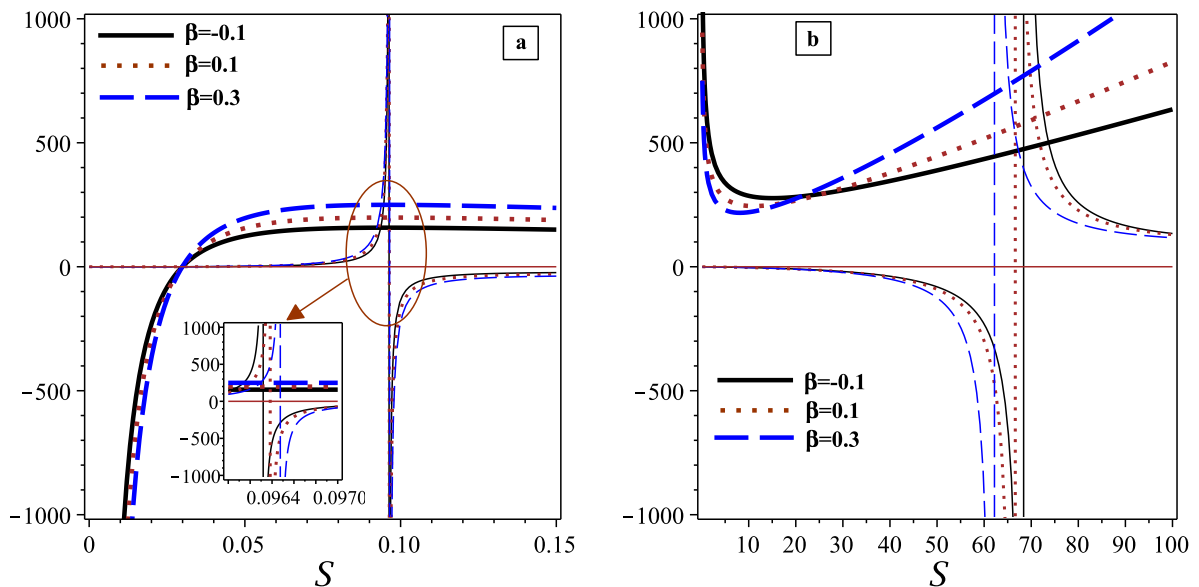


FIG. 3: The heat capacity ( $C_Q$ ) and the Hawking temperature ( $T$ ) versus entropy ( $S$ ) for different values of  $\beta$  by considering  $Q = b = -\eta_2 = 0.1$ ,  $\alpha = 0.3$ ,  $\eta_1 = 0.5$ ,  $\Lambda = -0.1$ ,  $c_0 = 1$ , and  $m_g = 0.2$ . Bold lines represent the Hawking temperature ( $T$ ), while thin lines indicate the heat capacity ( $C_Q$ )

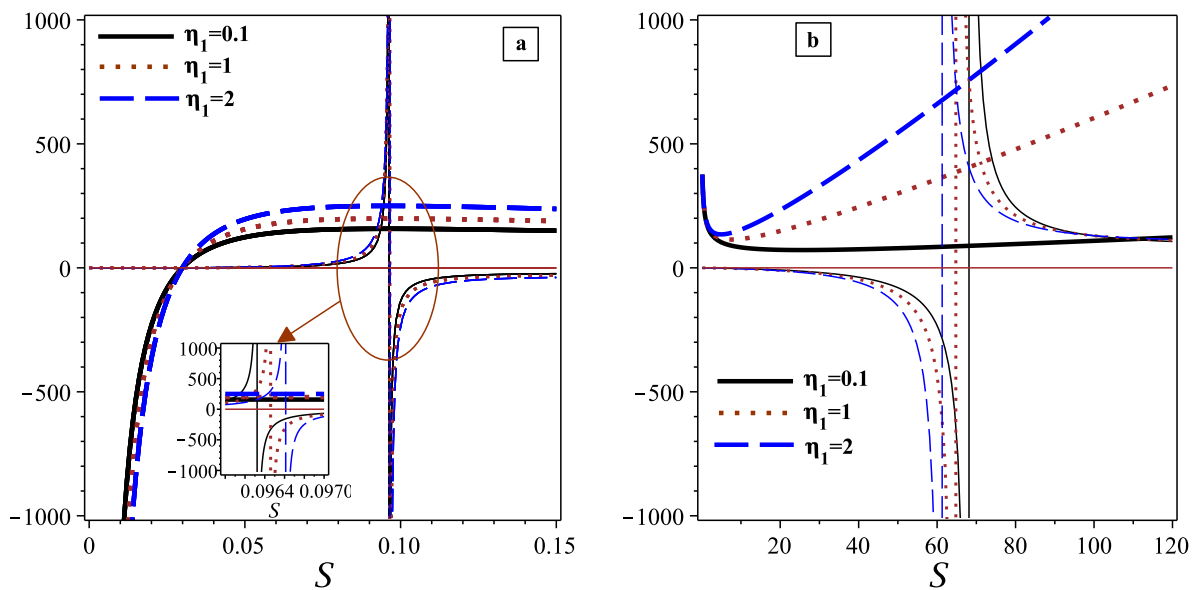


FIG. 4: The heat capacity ( $C_Q$ ) and the Hawking temperature ( $T$ ) versus entropy ( $S$ ) for different values of  $\eta_1$  by considering  $Q = b = \beta = -\eta_2 = 0.1$ ,  $\alpha = 0.3$ ,  $\Lambda = -0.1$ ,  $c_0 = 1$ , and  $m_g = 0.2$ . Bold lines represent the Hawking temperature ( $T$ ), while thin lines indicate the heat capacity ( $C_Q$ )

resembles that of a van der Waals fluid. Specifically, when the charge is below a critical value, the isocharge in the temperature-entropy plane exhibits one unstable branch and two stable branches, along with a second-order critical point at a critical charge. Consequently, we observe a van der Waals-like phase transition in charged black holes within dilaton-dRGT-like massive gravity. This behavior has been documented in Ref. [116], which explores the extended phase space by treating the cosmological constant as thermodynamic pressure ( $P = -\frac{\Lambda}{8\pi}$ ) [117–122], with its conjugate

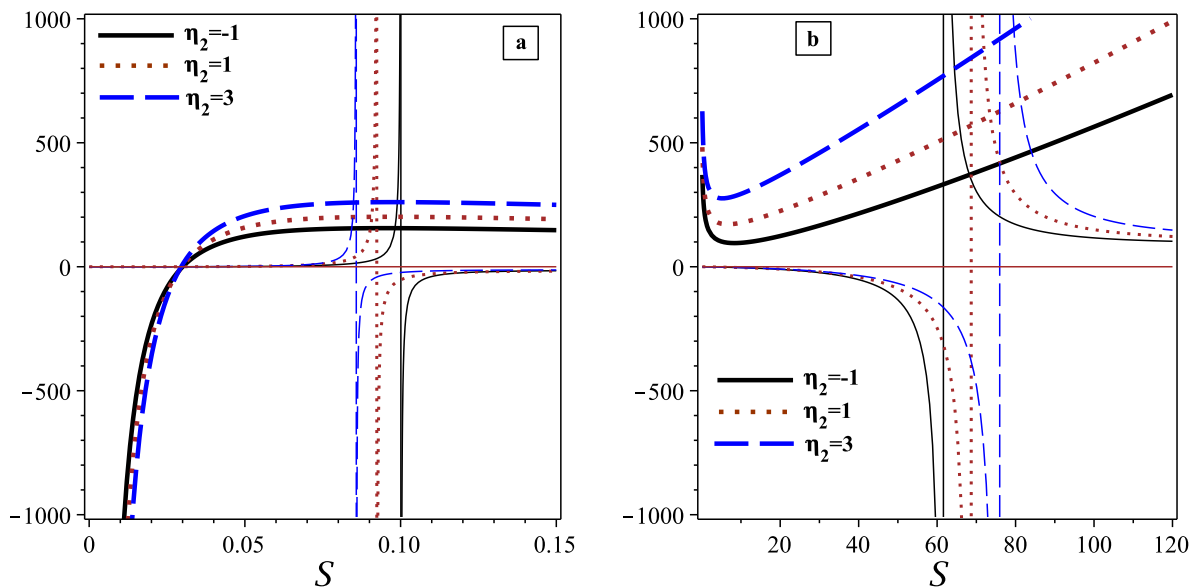


FIG. 5: The heat capacity ( $C_Q$ ) and the Hawking temperature ( $T$ ) versus entropy ( $S$ ) for different values of  $\eta_2$  by considering  $Q = b = \beta = 0.1$ ,  $\eta_1 = 1$ ,  $\alpha = 0.3$ ,  $\Lambda = -0.1$ ,  $c_0 = 1$ , and  $m_g = 0.2$ . Bold lines represent the Hawking temperature ( $T$ ), while thin lines indicate the heat capacity ( $C_Q$ )

quantity considered as thermodynamic volume. Under this framework, a distinct pressure-volume oscillatory behavior emerges, linking the small-large black hole phase transition to the liquid-gas phase transition of the van der Waals fluid [123]. This phenomenon has been further investigated in detail for black holes in Refs. [124–130].

As we mentioned in the previous paragraph, the phase transition of Maxwell-dilaton-dRGT-like black holes have been examined in greater detail in Ref. [116]. The authors evaluated the effects of the parameters  $\alpha$  and  $\gamma$  on the phase transition within both canonical and grand canonical ensembles. Specifically, they found that, when considering black holes in the context of dilaton-dRGT-like massive gravity and under grand canonical ensembles, van der Waals-like critical behavior necessitates a coupling between the graviton and dilaton fields ( $\gamma \neq 0$ ). Furthermore, when  $\alpha \neq 0$ , additional phenomena emerge, potentially including first-order phase transitions between small black holes (SBHs) and large black holes (LBHs). An analysis of the Gibbs free energy indicates the presence of a triple critical point and a zero-order reverse reentrant phase transition (SBHs  $\leftrightarrow$  LBHs  $\leftrightarrow$  SBHs), which is thermodynamically the opposite of the standard reentrant transition. In contrast, in canonical ensembles, van der Waals-like transitions can occur without coupling; however, an examination of the Helmholtz free energy also reveals that reverse reentrant transitions exist when  $\alpha \neq 0$ . In the context of the phase transition in the canonical ensemble, we examined the heat capacity in greater detail. We found that black holes in the Maxwell-dilaton-dRGT-like massive theory can undergo a phase transition between small black holes (SBHs) and large black holes (LBHs). Our findings are consistent with the results obtained in Ref. [131] within the canonical ensemble.

### C. Geometrothermodynamics

Geometrothermodynamics offers a valuable approach for exploring the critical points of phase transitions, specifically the divergence points of heat capacity in black holes. Historically, several thermodynamic metrics have been developed to identify these critical points, including those proposed by Weinhold [132, 133], Ruppeiner [134, 135], Quevedo [136, 137], and HPEM [138]. However, references indicate that the Ruppeiner, Weinhold, and Quevedo metrics may not fully align with all divergence and zero points of heat capacity for certain black holes [139, 140]. In contrast, there have been no reported inconsistencies with the HPEM metric regarding the identification of these divergence points and zero heat capacity. In this study, we will examine four thermodynamic metrics to determine which one accurately corresponds to the divergence and zero points of heat capacity in charged black holes within the framework of dilaton-dRGT-like massive gravity.

The Weinhold metric is introduced as follows [132, 133]

$$ds_W^2 = g_{ab}^W dX^a dX^b, \quad (37)$$

where  $g_{ab}^W = \frac{\partial^2 M(X^c)}{\partial X^a \partial X^b}$  and  $X^a \equiv X^a(S, N^i)$ , with  $N^i$  representing other extensive variables of the system.

Using the metric (37), we can express the denominator of Weinhold's Ricci scalar for charged black holes in dilaton-dRGT-like massive gravity as follows

$$\text{denom}(R_W) = (M_{SS}M_{QQ} - M_{SQ}^2)^2 M^2, \quad (38)$$

where  $M = M(S, Q)$ . Comparing Eq. (29) and Eq. (38), we observe that the denominator of the Weinhold Ricci scalar contains two additional terms,  $M_{SQ}^2$  and  $M_{QQ}$ . These extra terms create a mismatch between the divergence and zero points of the heat capacity and the divergences of the Weinhold Ricci scalar. Consequently, the Weinhold metric exhibits additional divergences that are not associated with any bounds or phase transition points of the heat capacity.

For further details, we present a plot of the heat capacity and the Ricci scalar of the Weinhold metric versus entropy in Fig. 6. Our findings indicate that the physical limitations (roots of the heat capacity) and the critical points of phase transitions (divergence points of heat capacity) do not coincide with the divergences of the Ricci scalar of the Weinhold metric.

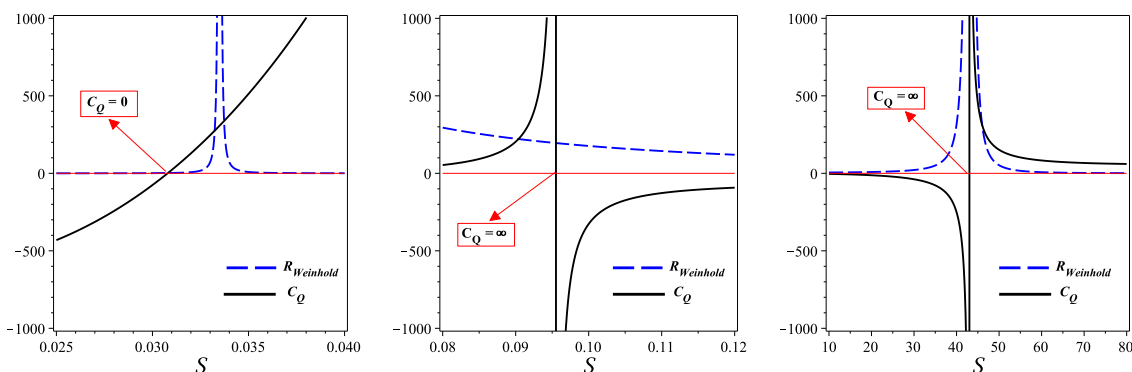


FIG. 6: The heat capacity ( $C_Q$ ) and the Ricci scalar of the Weinhold metric ( $R_{Weinhold}$ ) versus entropy ( $S$ ) for  $Q = b = \beta = -\eta_2 = 0.1$ ,  $\eta_1 = 0.5$ ,  $\Lambda = -0.1$ ,  $c_0 = 1$ , and  $m_g = \alpha = 0.2$ . Continuous line corresponds to the heat capacity ( $C_Q$ ), while the dashed line represents the Ricci scalar of the Weinhold metric ( $R_{Weinhold}$ )

The Ruppeiner metric is defined as follows [134, 135]

$$ds_R^2 = \frac{1}{T} ds_W^2, \quad (39)$$

where the metrics of Ruppeiner and Weinhold are conformally equivalent, with the inverse of the temperature serving as the conformal factor.

Considering equation (39), we derive the denominator of Ruppeiner's Ricci scalar for charged black holes in dilaton-dRGT-like massive gravity as follows

$$\text{denom}(R_R) = (M_{SS}M_{QQ} - M_{SQ}^2)^2 M^2 T, \quad (40)$$

where  $T = T(S, Q)$ . Like the Weinhold metric, the Ruppeiner Ricci scalar includes two additional terms in its denominator ( $M_{SQ}^2$  and  $M_{QQ}$ ) that do not correspond to any bounds or phase transition points of the heat capacity. As a result, this metric cannot fully capture the phase transitions and bound points of certain thermodynamic systems due to these extra terms in the denominator.

To investigate the behavior of the Ruppeiner metric, we plot the heat capacity and the Ricci scalar of the Ruppeiner metric versus entropy in Fig. 7. Our findings show that the physical limitations and the critical points of phase transitions do not coincide with the divergences of the Ricci scalar of the Ruppeiner metric.

The Quevedo metric is given by [136, 137]

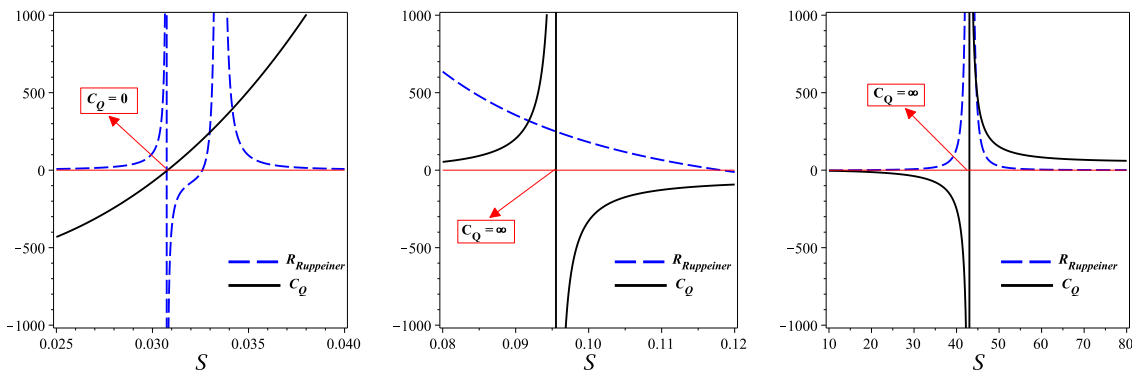


FIG. 7: The heat capacity ( $C_Q$ ) and the Ricci scalar of the Ruppeiner metric ( $R_{Ruppeiner}$ ) versus entropy ( $S$ ) for  $Q = b = \beta = -\eta_2 = 0.1$ ,  $\eta_1 = 0.5$ ,  $\Lambda = -0.1$ ,  $c_0 = 1$ , and  $m_g = \alpha = 0.2$ . Continuous line corresponds to the heat capacity ( $C_Q$ ), while the dashed line represents the Ricci scalar of the Ruppeiner metric ( $R_{Ruppeiner}$ )

$$ds_Q^2 = \Omega (-M_{SS}dS^2 + M_{QQ}dQ^2), \quad (41)$$

where  $M_{QQ} = \left(\frac{\partial^2 M(S,Q)}{\partial Q^2}\right)_S$ , and  $\Omega$  is

$$\Omega = \begin{cases} SM_S + QM_Q & \text{case I} \\ SM_S & \text{case II} \end{cases}. \quad (42)$$

Applying the Quevedo metrics (41), we can extract the denominator of Quevedo's Ricci scalar for charged black holes in dilaton-dRGT-like massive gravity, which leads to

$$\text{denom}(R_Q) = \begin{cases} (SM_S + QM_Q)^3 M_{SS}^2 M_{QQ}^2 & \text{case I} \\ S^3 M_S^3 M_{SS}^2 M_{QQ}^2 & \text{case II} \end{cases}. \quad (43)$$

Due to the presence of  $M_Q = \left(\frac{\partial M(S,Q)}{\partial Q}\right)_S$  and  $M_{QQ}^2$  in Quevedo's Ricci scalars, we may encounter additional divergence points that do not correspond to the phase transition or the critical points of the heat capacity. For further details, we plot this metric versus entropy in Fig. 8. As shown in the left panel of Fig. 8, there are no divergence points of Quevedo's Ricci scalar that coincide with the zero point of the heat capacity.

The HPEM metric is introduced in reference [138] as

$$dS_{HPEM}^2 = \frac{SM_S}{M_{QQ}^3} (-M_{SS}dS^2 + M_{QQ}dQ^2). \quad (44)$$

We derive the denominator of HPEM's Ricci scalar for charged black holes in dilaton-dRGT-like massive gravity as follows

$$\text{denom}(R_{HPEM}) = S^3 M_S^3 M_{SS}^2, \quad (45)$$

this ensures that all phase transition and bound points align with the divergences of the HPEM's Ricci scalar, without introducing any additional terms that could create extra divergences.

Our findings indicate that the divergence points of the Ricci scalar of the HPEM metric coincides with both the roots and divergence points of the heat capacity. For further details, please refer to Fig. 9. This means that all physical limitations (roots of the heat capacity) and the critical points of phase transitions (divergence points of heat capacity) are reflected in the divergences of the Ricci scalar of the HPEM metric (see Fig. 9). Another important result concerning the HPEM metric is the differing behavior of the Ricci scalar before and after its divergence points.

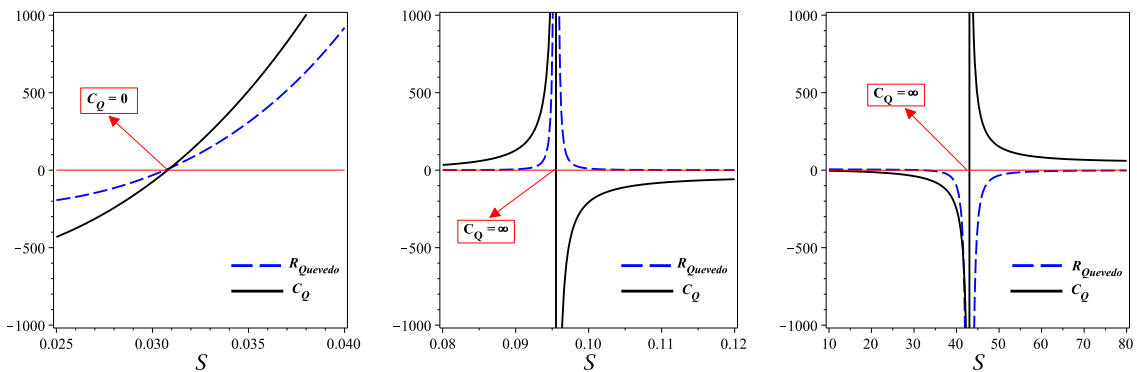


FIG. 8: The heat capacity ( $C_Q$ ) and the Ricci scalar of the Quevedo metric ( $R_{Quevedo}$ ) versus entropy ( $S$ ) for  $Q = b = \beta = -\eta_2 = 0.1$ ,  $\eta_1 = 0.5$ ,  $\Lambda = -0.1$ ,  $c_0 = 1$ , and  $m_g = \alpha = 0.2$ . Continuous line corresponds to the heat capacity ( $C_Q$ ), while the dashed line represents the Ricci scalar of the Quevedo metric ( $R_{Quevedo}$ )

Specifically, the Ricci scalar exhibits distinct behavior at divergence points associated with physical limitations and phase transition critical points. In other words, the sign of the Ricci scalar changes before and after divergences when the heat capacity is zero (see Fig. 9). However, the signs of the Ricci scalar remain the same when the heat capacity encounters divergences (see Fig. 9). These divergences are referred to as  $\Lambda$  divergences. Therefore, this approach allows us to differentiate between physical limitations and phase transition critical points.

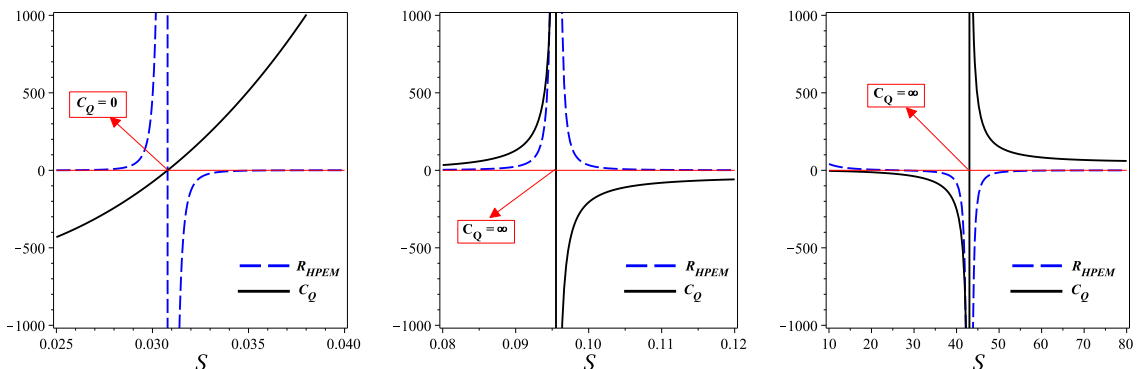


FIG. 9: The heat capacity ( $C_Q$ ) and the Ricci scalar of the HPEM metric ( $R_{HPEM}$ ) versus entropy ( $S$ ) for  $Q = b = \beta = -\eta_2 = 0.1$ ,  $\eta_1 = 0.5$ ,  $\Lambda = -0.1$ ,  $c_0 = 1$ , and  $m_g = \alpha = 0.2$ . Continuous line corresponds to the heat capacity ( $C_Q$ ), while the dashed line represents the Ricci scalar of the HPEM metric ( $R_{HPEM}$ )

#### IV. OPTICAL FEATURES

The groundbreaking image of a black hole captured by the Event Horizon Telescope [141, 142] has highlighted the significance of studying shadow phenomena and geodesic structures for a deeper understanding of black hole characteristics [143–151]. This study focuses on deriving null geodesic equations and investigating how Maxwell-dilaton-dRGT-like massive gravity influences photon trajectories through Lagrangian formalism in the following sections.

##### A. Photonic radius

In this part, we examine the photonic radius in the Maxwell-dilaton-dRGT-like massive framework. The Lagrangian is defined as  $2\mathcal{L} = g_{\mu\nu}\dot{x}^\mu\dot{x}^\nu$ , and the dot denotes differentiation concerning an arbitrary affine parameter. Assuming

motion is confined to the equatorial plane, i.e.,  $\theta = \frac{\pi}{2}$ , the Lagrangian for a photon as a massless particle simplifies to

$$2\mathcal{L} = -f(r)\dot{t}^2 + \frac{\dot{r}^2}{f(r)} + r^2 R^2(r)\dot{\phi}^2 = 0. \quad (46)$$

Moreover, the presence of two Killing vectors within the system results in two conserved quantities: energy, denoted as  $E = f(r)\dot{t}$ , and angular momentum, represented as  $L = r^2 R^2(r)\dot{\phi}$ . Considering these assumptions, Eq. (46) leads to the radial equation

$$\dot{r}^2 + E^2 = V_{\text{eff}}, \quad (47)$$

where the effective potential is expressed as

$$V_{\text{eff}} = \frac{L^2 f(r)}{r^2 R^2(r)}. \quad (48)$$

The photonic radius  $r_{\text{ph}}$  is calculated by finding the critical radius in the effective potential

$$V_{\text{eff}} = \frac{\partial V_{\text{eff}}}{\partial r} = 0, \quad (49)$$

The unstable critical orbits determine the photonic radius  $r = r_{\text{ph}}$ , which can be found by the sign of the second derivative of the effective potential. For an unstable critical orbit (which is the physically relevant case for black hole photon spheres), the following condition must be satisfied.

$$\left. \frac{\partial^2 V_{\text{eff}}}{\partial r^2} \right|_{r=r_{\text{ph}}} < 0 \quad (50)$$

Fig. 10 shows the typical shape of  $V_{\text{eff}}$  for fixed parameters at  $m_0 = 0.5$ ;  $\alpha = b_0 = \beta = q = -\eta_2 = -\Lambda = m_g = 0.1$ ;  $c_0 = \eta_1 = 1$  and  $L = 6$ . The plot demonstrates clearly that  $r_{\text{ph}}$  corresponds to a local maximum, confirming the unstable nature of the photon orbits.

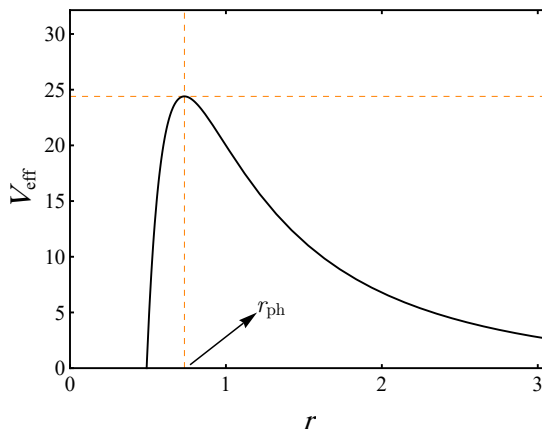


FIG. 10: Typical shape of the effective potential  $V_{\text{eff}}(r)$  for null geodesics, showing a maximum at the photon sphere

radius  $r = r_{\text{ph}}$ . The condition  $\left. \frac{\partial^2 V_{\text{eff}}}{\partial r^2} \right|_{r=r_{\text{ph}}} < 0$  confirms the instability of photon orbits at this radius.

Now, we calculate the photonic radius by utilizing Eq. (49), which leads to the following equation

$$r_{\text{ph}} \left( (\alpha^2 + 1) \left( c_0 m_g^2 \left( \frac{b}{r_{\text{ph}}} \right) - \frac{2\alpha\beta}{\alpha^2 + 1} \left( -\frac{\eta_1 r_{\text{ph}} \left( \frac{b}{r_{\text{ph}}} \right)^{\frac{\alpha^2}{\alpha^2 + 1}}}{\alpha^2 + 2\alpha\beta + 2} - \frac{2c_0\eta_2}{\alpha^2 + 2\alpha\beta - 1} \right) - \frac{4q^2 \left( \frac{b}{r_{\text{ph}}} \right)^{\frac{\alpha^2}{\alpha^2 + 1}}}{(\alpha^2 - 1)b^2} \right) - 2 \right) - \frac{(\alpha^2 - 3)m_0 b^{\frac{2\alpha^2}{\alpha^2 + 1}}}{\alpha^2 + 1} = 0. \quad (51)$$

Table I presents the dependence of the photonic radius  $r_{\text{ph}}$  on the key parameters: the parameters of the dilaton field ( $\alpha$ ), massive gravity parameter ( $\eta_1$ ), charge ( $q$ ) and also the graviton mass ( $m_g$ ) in the framework of Maxwell-dilaton-dRGT-like massive gravity, with all other variables held constant on  $m_0 = 0.5$ ,  $b_0 = 0.1$ ,  $c_0 = 1$ ,  $\eta_2 = -0.1$ ,  $\beta = 0.1$ , and  $q = 0.1$ . It is worth mentioning that the photonic radius is independent of the cosmological constant based on Eq. ((51)). The results offer valuable insights into how these physical quantities influence the behavior of photon orbits around black holes.

Based on Eq. (10) and the discussion in Sec. II, the spacetime structure is governed by several key parameters, whose variations can significantly influence its physical characteristics. Accordingly, when deriving a general expression, particular attention must be paid to the behavior of parameters. The results presented here have been obtained for a specific set of parameter values, and while they effectively illustrate the underlying physical features, their applicability should be regarded as limited to this chosen parameter regime.

Table I summarizes the behavior of the photon radius  $r_{\text{ph}}$  for different choices of the dilaton field parameter  $\alpha$ , the graviton mass  $m_g$ , the electric charge  $q$ , and the parameter  $\eta_1$ . The corresponding trends are interpreted below.

- **Dilaton field ( $\alpha$ ):** Starting with the variation of the dilaton field parameter  $\alpha$ , for fixed  $\eta_1 = -2$ ,  $q = 0.5$ , and  $m_g = 0.2$ , Table I shows that  $r_{\text{ph}}$  decreases as  $\alpha$  increases. This trend reflects the role of the dilaton field in strengthening the effective gravitational attraction near the horizon. A larger  $\alpha$  enhances the coupling between the scalar and electromagnetic sectors, effectively deepening the potential well and drawing the photon orbit closer to the black hole. Consequently, the photon sphere becomes more compact for a stronger dilaton field.
- **Graviton mass ( $m_g$ ):** In contrast to the role of  $\alpha$ , an opposite behavior is observed when varying the graviton mass  $m_g$  while keeping  $\alpha = 0.1$ ,  $q = 0.5$ , and  $\eta_1 = -2$  fixed. The photon radius  $r_{\text{ph}}$  increases with increasing  $m_g$ . Physically, this can be attributed to the modification of spacetime curvature introduced by the massive graviton term. A higher graviton mass effectively weakens the gravitational field at a given radius, reducing the overall curvature strength and allowing the photon sphere to extend outward.
- **Electric charge ( $q$ ):** The influence of the charge parameter  $q$  is also evident from Table I when  $\alpha = 0.1$ ,  $m_g = 0.2$ , and  $\eta_1 = -2$  are held constant. Here,  $r_{\text{ph}}$  grows with increasing  $q$ . This arises from the repulsive contribution of the electromagnetic field, which counteracts the gravitational attraction. As the electric charge increases, the net potential barrier moves outward, resulting in a larger photon sphere radius.
- **Massive gravity parameter ( $\eta_1$ ):** Finally, the parameter  $\eta_1$  exerts an opposite effect. For fixed  $\alpha = 0.1$ ,  $m_g = 0.2$ , and  $q = 0.5$ , higher values of  $\eta_1$  lead to smaller  $r_{\text{ph}}$ . This indicates that positive  $\eta_1$  strengthens the attractive component of the massive gravity potential, effectively confining photons more tightly near the black hole.

Overall, these trends highlight the delicate interplay among the dilaton field, electromagnetic charge, and massive gravity effects in shaping the photon sphere structure. The variation of  $r_{\text{ph}}$  with different parameters provides valuable insights into how scalar, vector, and tensor degrees of freedom collectively influence the near-horizon geometry in the Maxwell-dilaton-dRGT-like massive gravity framework. The dependence of the photonic radius on these parameters will, in turn, have direct implications for observable features such as the black hole shadow, which will be examined in the following section.

TABLE I: Variation of the photon radius  $r_{\text{ph}}$  with respect to the model parameters  $\alpha$ ,  $m_g$ ,  $q$ , and  $\eta_1$  in the Maxwell-dilaton-dRGT-like massive gravity background. The photonic radius is computed for specific parameters set to fixed values;  $m_0 = 1$ ,  $b = 0.2$ ,  $\beta = 0.15$ ,  $\eta_2 = -0.1$ ,  $\Lambda = -0.1$ , and  $c_0 = 1$ .

$\alpha$	0.00	0.05	0.10	0.15	0.20	0.25	0.30
$r_{\text{ph}}$	1.8327	1.8220	1.7896	1.7413	1.6858	1.6331	1.5935
$m_g$	0.0	0.2	0.4	0.6	0.8	1.0	1.2
$r_{\text{ph}}$	1.7398	1.7427	1.7517	1.7670	1.7896	1.8208	1.8627
$q$	0.0	0.1	0.2	0.3	0.4	0.5	0.6
$r_{\text{ph}}$	1.4718	1.4870	1.5307	1.5990	1.6869	1.7896	1.9037
$\eta_1$	-3	-2	-1	0	+1	+2	+3
$r_{\text{ph}}$	1.8211	1.7896	1.7604	1.7332	1.7077	1.6837	1.6611

## B. Shadow radius

Once the photon sphere radius  $r_{\text{ph}}$  has been determined, we can proceed to evaluate the corresponding shadow radius. For a spacetime expressed as  $ds^2 = -g_{tt}dt^2 + g_{rr}dr^2 + g_{\theta\theta}d\theta^2 + g_{\varphi\varphi}d\varphi^2$ , the angular size of shadow  $\alpha_{\text{sh}}$  is assumed with the following expression [143]

$$\sin \alpha_{\text{sh}} = \frac{h(r_{\text{ph}})}{h(r_{\text{O}})}, \quad (52)$$

where  $h(r)$  is defined as

$$h(r)^2 = \frac{g_{\varphi\varphi}}{g_{tt}} = \frac{r^2 R^2(r)}{f(r)}. \quad (53)$$

and based on Eq. (52), the shadow radius detected by an observer located at  $\tilde{r}_{\text{O}}$  is approximately defined by

$$\alpha_{\text{sh}} \approx \frac{\mathcal{R}_{\text{sh}}}{\tilde{r}_{\text{O}}}. \quad (54)$$

By utilizing the definition of  $h(r)$  in Eq. (53) and the photonic radius obtained by Eq. (51), we explore the shadow radius with the help of the following equation

$$\mathcal{R}_{\text{sh}} = \frac{r_{\text{ph}} R(r_{\text{ph}})}{\sqrt{f(r_{\text{ph}})}} \sqrt{f(r_{\text{O}})}. \quad (55)$$

As the shadow radius  $\mathcal{R}_{\text{sh}}$  is a key observable that characterizes the apparent size of a black hole's dark silhouette against the background light. We now analyze its dependence on the parameters of our Maxwell-dilaton-dRGT-like massive gravity model. The behavior of  $\mathcal{R}_{\text{sh}}$ , plotted in the celestial coordinates  $\xi$  and  $\eta$  [143, 152], as a function of the model parameters in Figs. 11. In these figures, the shadow size is calculated for a distant observer, and its dependence on the parameters  $\alpha$ ,  $m_g$ ,  $q$ , and  $\eta_1$  reflects the underlying modifications to the spacetime geometry. The analysis for each parameter was conducted by varying it while keeping the others fixed at the following baseline values:  $m_0 = 1$ ,  $b = 0.2$ ,  $\beta = 0.15$ ,  $\eta_2 = -0.1$ ,  $\Lambda = -0.1$ , and  $c_0 = 1$ .

- **Dilaton field ( $\alpha$ ):** The upper-left panel of Fig. 11 illustrates the dependence of the shadow radius  $\mathcal{R}_{\text{sh}}$  on the dilaton field parameter  $\alpha$  for fixed values  $m_g = 0.1$ ,  $\eta_1 = -1$ , and  $q = 0.7$ . It is evident that  $\mathcal{R}_{\text{sh}}$  **decreases** as  $\alpha$  increases. This trend parallels the reduction of the photon sphere radius  $r_{\text{ph}}$ , as a stronger dilaton field enhances the coupling between the scalar and electromagnetic sectors. Consequently, the effective gravitational potential near the horizon deepens, leading to a more tightly bound photon orbit and a smaller apparent shadow. In this sense, the dilaton field acts to concentrate the spacetime curvature, resulting in a more compact shadow profile.
- **Graviton mass ( $m_g$ ):** The upper-right panel of Fig. 11 displays the behavior of  $\mathcal{R}_{\text{sh}}$  with respect to the graviton mass, for  $\alpha = 0.1$ ,  $\eta_1 = -2$ , and  $q = 0.7$ . The shadow radius **increases** as  $m_g$  grows. This is consistent with the outward displacement of  $r_{\text{ph}}$  observed earlier. Physically, the introduction of a finite graviton mass modifies the curvature of spacetime, effectively weakening the central gravitational pull. As a result, photons can orbit at larger radii, and the corresponding shadow appears larger. This behavior highlights the role of massive gravity terms in altering the effective lensing geometry of the black hole.
- **Electric charge ( $q$ ):** The lower-left panel of Fig. 11 examines the impact of the electric charge for fixed parameters  $\alpha = 0.1$ ,  $m_g = 0.2$ , and  $\eta_1 = -2$ . The shadow radius **increases** with increasing  $q$ . This outcome aligns with the behavior of  $r_{\text{ph}}$ , where the repulsive electromagnetic interaction counteracts the gravitational attraction. As  $q$  increases, the balance between these two effects shifts outward, allowing photons to orbit farther from the black hole. Consequently, the shadow expands, reflecting the reduced effective curvature of the surrounding spacetime.
- **Massive gravity parameter ( $\eta_1$ ):** Finally, the lower-right panel of Fig. 11 shows that  $\mathcal{R}_{\text{sh}}$  **decreases** as  $\eta_1$  increases, for  $\alpha = 0.1$ ,  $m_g = 0.2$ , and  $q = 0.7$ . This behavior underscores the role of  $\eta_1$  in strengthening the attractive component of the massive gravity potential. A larger  $\eta_1$  enhances the effective gravitational pull, confining photons to tighter orbits and reducing the shadow size. The dependence of  $\mathcal{R}_{\text{sh}}$  on  $\eta_1$  thus provides a direct probe of how massive gravity corrections influence the strong-field region around the black hole.

The results align with and visually confirm the trends previously established for the photon orbit radius  $r_{\text{ph}}$  in Table I. In summary, the shadow radius  $\mathcal{R}_{\text{sh}}$  exhibits a direct correlation with the photon orbit radius  $r_{\text{ph}}$ . Parameters that cause  $r_{\text{ph}}$  to increase ( $m_g, q$ ) result in a larger shadow, while those that cause it to decrease ( $\alpha, \eta_1$ ) result in a smaller one.

It is worth emphasizing that the above results illustrate the characteristic influence of each parameter when the remaining quantities are fixed. In the Maxwell–dilaton–dRGT-like massive gravity framework, these parameters are not entirely independent, and their effects can interplay in nontrivial ways. Variations in one parameter may partially compensate or amplify the influence of another, leading to different quantitative outcomes. Therefore, while the present analysis captures the dominant trends for representative parameter choices, the precise behavior of the shadow radius and photon sphere may vary under alternative parameter sets. A more exhaustive exploration of the multi-parameter space could thus reveal richer structures in the black hole’s optical appearance and gravitational lensing properties as a potential research project in the future studies.

Nevertheless, the present results clearly demonstrate that the combined effects of the dilaton field, electromagnetic charge, and massive gravity sector play a decisive role in shaping the black hole’s shadow. These interrelated contributions give rise to distinct modifications in the shadow geometry, offering potential observational signatures that can be employed to test and constrain such extended gravity models. The next section is devoted to comparing the theoretical predictions for the shadow radius with available observational data.

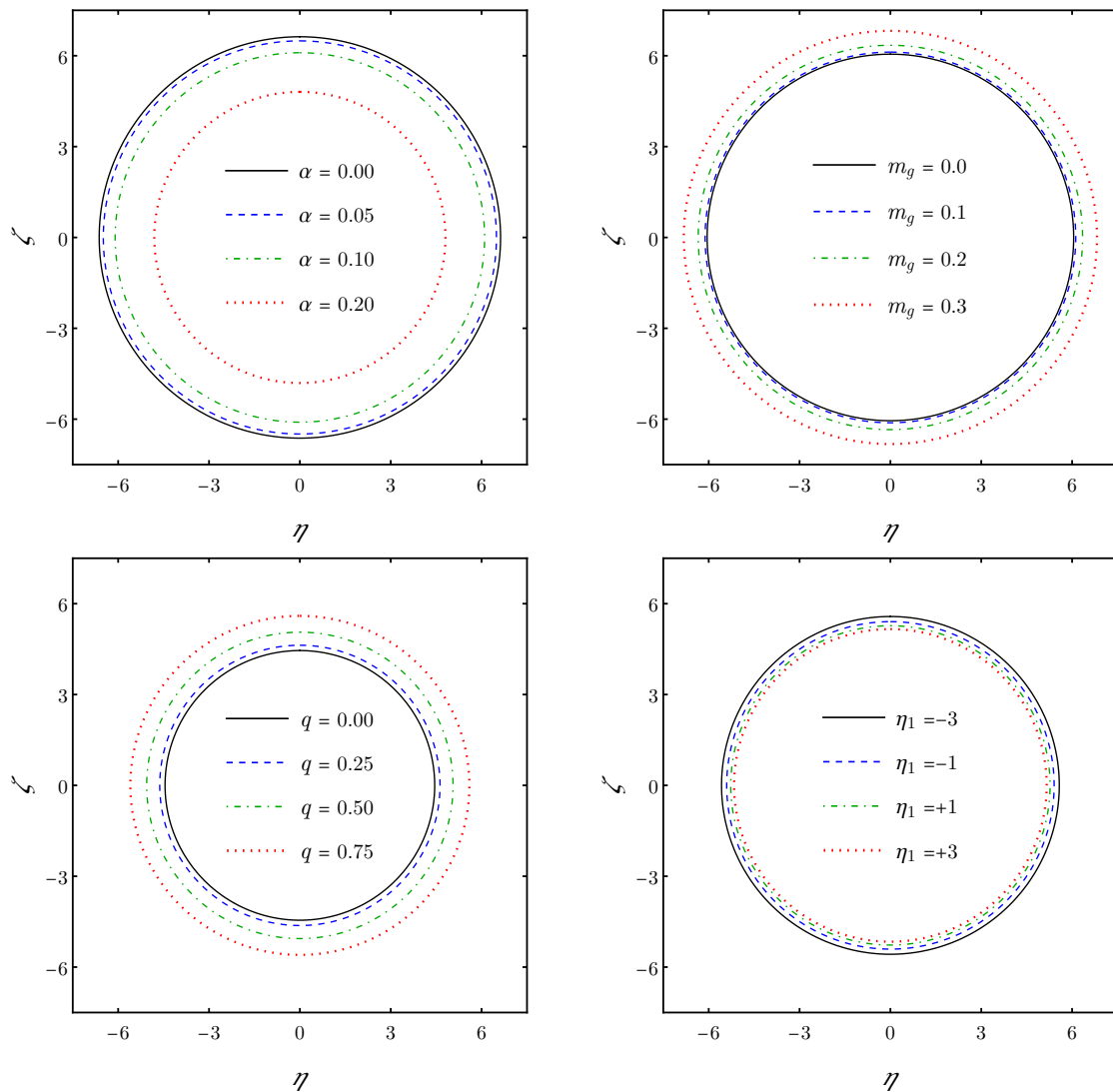


FIG. 11: The shadow radius  $\mathcal{R}_{\text{sh}}$  as a function of the model parameters in Maxwell-dilaton-dRGT-like massive gravity. The following fixed parameters are used for all plots:  $m_0 = 1$ ,  $b = 0.2$ ,  $c_0 = 1$ ,  $\eta_2 = -0.1$ ,  $\Lambda = -0.1$ ,  $\beta = 0.15$ , and the observer radius is set at  $r_{\text{O}} = 10$ .

## V. CONSTRAINTS FROM THE EHT OBSERVATION OF EHT

The Event Horizon Telescope (EHT) observations of black hole shadows have placed powerful constraints on alternative theories of gravity and provided deep insight into the structure of spacetime in the strong-field regime. In the context of the Maxwell-dilaton-dRGT-like massive gravity framework, these data offer an opportunity to examine how the combined effects of the dilaton field, electromagnetic coupling, and graviton mass influence the observable shadow. In this section, we aim to estimate the range of admissible model parameters consistent with the EHT results for  $SgrA^*$ .

To perform this comparison, an accurate mass-to-distance ratio for  $SgrA^*$  is required. Independent determinations from the Keck [153] and GRAVITY/VLTI [154] collaborations have provided consistent measurements of both quantities. Another key aspect is the calibration connecting the observed bright emission ring to the theoretical black hole shadow, which establishes how reliably the observed angular size can be used to infer the shadow boundary [145]. Combining this calibration with the uncertainties in the mass and distance estimates allows us to constrain the deviation between the observed and predicted shadow diameters.

According to the EHT collaboration [141], the angular diameter of the  $SgrA^*$  shadow is measured as  $48.7 \pm 7 \mu\text{as}$ . Using the averaged Keck and VLTI mass-to-distance priors, the following bounds on the dimensionless shadow radius are obtained [145, 155]

$$4.55 \lesssim \frac{\mathcal{R}_{\text{sh}}}{M} \lesssim 5.22 \quad (1\sigma), \quad (56)$$

and

$$4.21 \lesssim \frac{\mathcal{R}_{\text{sh}}}{M} \lesssim 5.56 \quad (2\sigma). \quad (57)$$

Figure 12 illustrates the variation of the shadow radius in mass units,  $\mathcal{R}_{\text{sh}}/M$ , as a function of the dilaton coupling parameter  $\alpha$  for several representative values of the charge  $q$ , the massive gravity parameter  $\eta_1$ , and the graviton mass  $m_g$  in the Maxwell-dilaton-dRGT-like massive gravity framework. The shaded green and blue regions represent the  $1\sigma$  and  $2\sigma$  observational intervals derived from the EHT image of Sgr A, corresponding to the measured shadow size range.

For each configuration, the intersection between the theoretical curves and the observational bounds specifies the range of  $\alpha$  values consistent with the EHT data. The allowed interval of  $\alpha$  varies noticeably with the other model parameters. As shown in the upper panel of Fig. 12, increasing the charge  $q$  slightly narrows the overlap region, shifting the allowed region toward the smaller  $\alpha$ , indicating that stronger electromagnetic effects reduce the parameter space in which the shadow agrees with observations. In the middle panel of Fig. 12, larger values of  $\eta_1$  shift the theoretical curves upward, thereby widening the overlap region with the observational bands. This trend implies that the influence of the massive gravity potential (through  $\eta_1$ ) permits a broader range of  $\alpha$  values consistent with Sgr A. In contrast, the down panel of Fig. 12 shows that increasing the graviton mass  $m_g$  leads to a downward shift of the theoretical curves, tightening the constraint on  $\alpha$  by increasing its lower bound and decreasing the upper one. This behavior suggests that stronger massive gravity effects suppress the shadow radius, restricting the viable range of the dilaton field.

These results demonstrate how the EHT measurement of  $SgrA^*$ 's shadow imposes meaningful constraints on the interplay between the dilaton field, electromagnetic charge, and massive gravity parameters. Within the parameter sets considered, the observationally allowed values of the dilaton field are confined, depending on the black hole parameters. While each constraints are derived for specific parameter choices, they capture the characteristic behavior of the Maxwell-dilaton-dRGT-like massive gravity model and provide a quantitative basis for confronting such theories with future high-precision shadow observations.

## VI. EMISSION RATE

In this section, we analyze the characteristics of the energy emission rate as a function of photon frequency. Quantum fluctuations near the event horizon of a black hole can give rise to the formation of particle-antiparticle pairs, which may escape the gravitational pull through a quantum tunneling mechanism, a process commonly referred to as Hawking radiation. This mechanism underpins the gradual loss of mass and the eventual evaporation of black holes over time. However, in many theoretical models, the black hole does not fully evaporate; instead, a nonzero remnant mass often remains. This remnant is of considerable interest, as it potentially preserves information that would otherwise be considered lost, thereby contributing to the resolution of the information loss paradox.

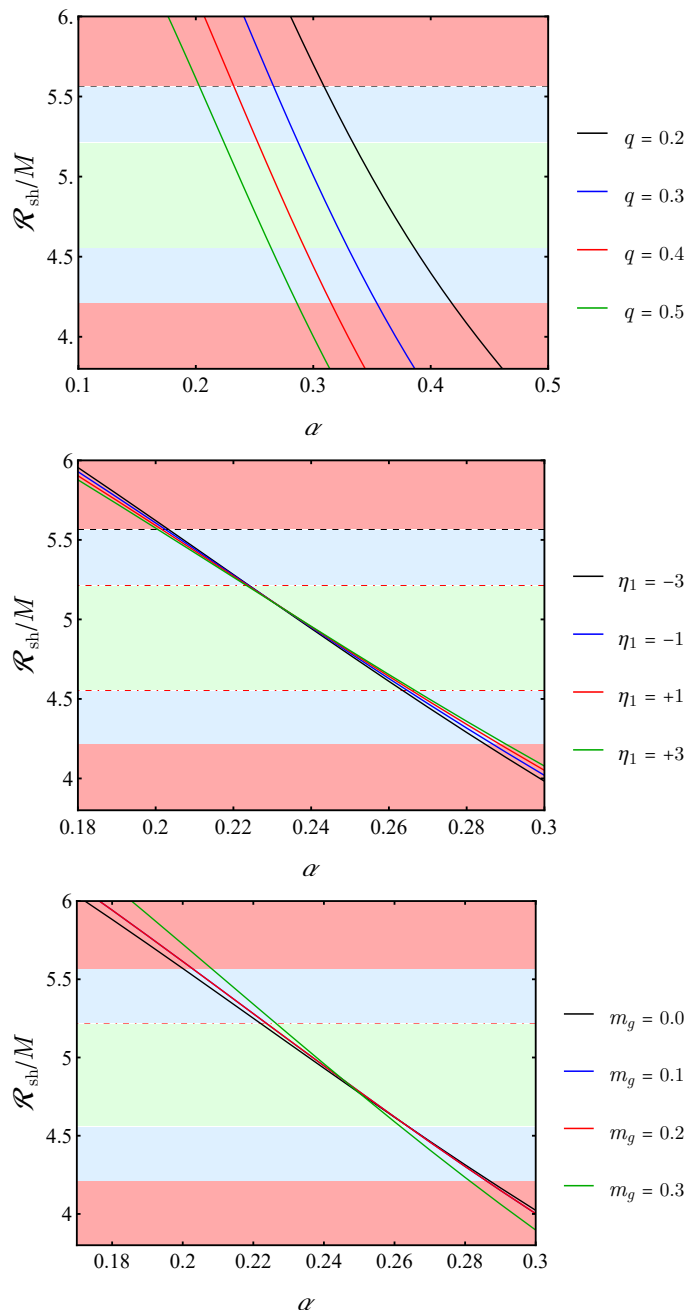


FIG. 12: The shadow radius  $\mathcal{R}_{\text{sh}}$  in the mass unit, as a function of the model parameters in Maxwell-dilaton-dRGT-like massive gravity. The following fixed parameters are used for all plots:  $m_0 = 1$ ,  $b = 0.2$ ,  $c_0 = 1$ ,  $\eta_2 = -0.1$ ,  $\Lambda = -0.1$ ,  $\beta = 0.15$ , and the observer radius is set at  $r_O = 10$ .

Following the framework presented in Refs. [156–158], the energy emission rate can be expressed as

$$\frac{d^2 E}{d\omega dt} = \frac{2\pi^2 \sigma \omega^3}{e^{\omega/T} - 1}, \quad (58)$$

where  $\omega$  denotes the photon frequency,  $T$  is the Hawking temperature shown in Eq. (22).  $\sigma$  is the absorption cross-section which approaches a constant value at high frequencies.  $\sigma$  is geometrically related to the black hole shadow radius  $\sigma_{\text{lim}} \approx \pi \mathcal{R}_{\text{sh}}^2$ . In Figs. 13, the energy emission rate is plotted as a function of the photon frequency  $\omega$  for various values of the parameters. The plots clearly exhibit a peak in the emission rate occurring at a particular frequency, indicating the most probable frequency for radiation emission. Furthermore, as inferred from the analytical

expression of the emission rate in Eq. (58), the intensity tends to vanish in both the low-frequency limit ( $\omega \rightarrow 0$ ) and the high-frequency limit ( $\omega \rightarrow \infty$ ).

The energy emission rate as a function of the photon frequency  $\omega$ , shown in Figs. 13, exhibits a distinct peak whose position and magnitude depend on the model parameters. In the upper-left panel, for  $m_g = 0.1$ ,  $\eta_1 = -1$ , and  $q = 0.7$ , increasing the dilaton field  $\alpha$  enhances the emission rate and shifts the peak toward higher frequencies. This indicates that, within the selected parameter range, the dilaton field can deepen the effective potential near the photon sphere, allowing more energetic photons to escape.

For fixed  $m_g = 0.1$ ,  $\eta_1 = -1$ , and  $\alpha = 0.1$ , a larger charge  $q$  significantly amplifies the emission peak, while the peak frequency remains nearly unchanged. This behavior may be attributed to the contribution of the electromagnetic field, which increases the overall energy release without substantially altering the effective temperature associated with photon emission.

When  $m_g = 0.1$ ,  $\alpha = 0.1$ , and  $q = 0.7$ , increasing  $\eta_1$  produces a higher and slightly blue-shifted peak, suggesting that this parameter modulates the massive gravity potential in a way that favors radiation escape from the near-horizon region. In contrast, for  $\alpha = 0.1$ ,  $\eta_1 = -1$ , and  $q = 0.5$ , a larger graviton mass  $m_g$  leads to a lower and red-shifted peak. This suppression can be interpreted as the massive gravity term increasing the effective curvature scale, thereby confining photons more strongly and reducing the efficiency of emission.

Overall, the trends show that  $\alpha$ ,  $q$ , and  $\eta_1$  tend to enhance high-frequency emission, whereas  $m_g$  suppresses it. These results collectively highlight the competing influences of the dilaton, electromagnetic, and massive gravity sectors on the radiation spectrum. It should be emphasized, however, that these interpretations are based on the chosen parameter sets and serve to illustrate the characteristic behavior within this specific regime of the Maxwell-dilaton-dRGT-like massive gravity model.

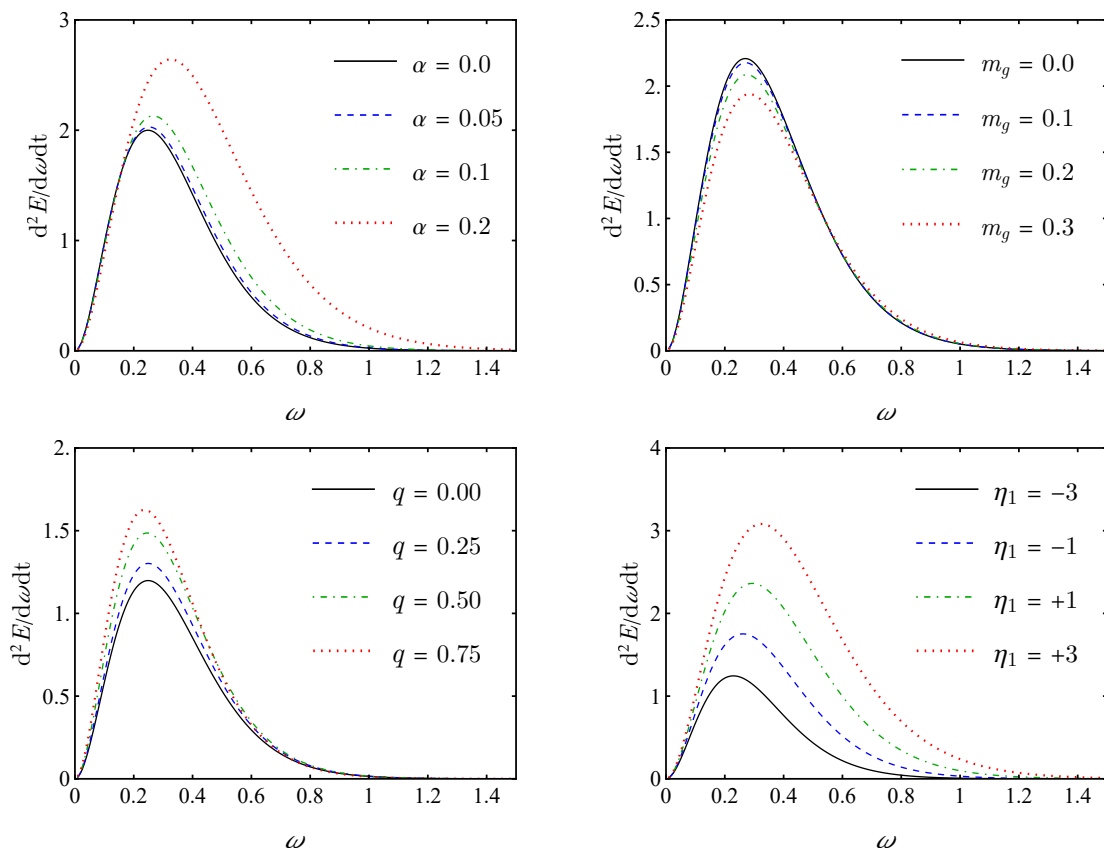


FIG. 13: Emission spectrum versus  $\omega$  for distinct values of the parameter set for all plots:  $m_0 = 1$ ,  $b = 0.2$ ,  $c_0 = 1$ ,  $\eta_2 = -0.1$ ,  $\Lambda = -0.1$ ,  $\beta = 0.15$ , and the observer radius is set at  $r_O = 10$ .

## VII. CONCLUSIONS

In this paper, we first reviewed charged black holes in dilaton-dRGT-like massive gravity. Then, we analyzed the asymptotic behavior of spacetime by adjusting the parameters of the dilaton field ( $\alpha$ ) and the coupling constant ( $\beta$ ). Our analysis indicated that: i) for all values of  $\alpha$ , the spacetime was not asymptotically (A)dS, and it depended on both  $\Lambda$  and  $\alpha$ ; ii) for  $\beta > \frac{-\gamma_2 - 1}{2\alpha}$ , the asymptotic behavior of the spacetime was determined by the cosmological constant, the parameters of the dilaton field, the parameters of the reference metric, and massive gravity ( $\eta_1$ ), as well as the graviton mass ( $m_g$ ); iii) for  $\alpha > -\beta$ , the asymptotic behavior of the spacetime depended on all parameters of the system. In addition, we studied the effects of mass, electrical charge, and the parameters  $\alpha$  and  $\beta$  on the metric function to find its roots. We found that these black holes could have multiple horizons, depending on the values of the various parameters. In other words, our findings revealed that there were critical values for the parameters of  $m_0$  (mass),  $q$  (electric charge),  $\alpha$ , and  $\beta$ , such that for less or more than these critical values, the charged black holes in dilaton-dRGT-like massive gravity encounter one, two, and three real roots. This was one of the interesting effects of massive gravity and the dilaton field on the roots of the metric function.

In the next section, we analyzed the conserved and thermodynamic quantities of charged black holes within dilaton-dRGT-like massive gravity. We examined how various parameters influenced the thermal stability areas and phase transition points by employing both heat capacity and geometrothermodynamics approaches. Our investigation into the heat capacity and temperature of these black holes revealed four distinct regions: very small and medium black holes were found to be non-physical and unstable, while small and large black holes met the conditions for physical and thermal stability. This indicated that small and large charged black holes in dilaton-dRGT-like massive gravity was indeed a physical and stable entity, facilitating a phase transition between the two sizes. Additionally, we assessed the effects of parameters  $\alpha$ ,  $\beta$ ,  $\eta_1$ , and  $\eta_2$  on these four regions. Our findings include:

- i) An increase in the dilaton field parameter ( $\alpha$ ) resulted in a reduction of the thermal stability area (see Fig. 2 for details).
- ii) The thermal stability areas expanded as the value of  $\beta$  increased (see Fig. 3 for details).
- iii) An increase in the dRGT-like massive gravity parameter ( $\eta_1$ ) led to an expansion of the thermal stability area (see Fig. 4 for details).
- iv) The thermal stability areas of these black holes decreased as  $\eta_2$  increased (see Fig. 5 for details).

Geometrothermodynamics provides an alternative method for exploring specific thermodynamic properties of black holes, particularly the critical points of phase transitions, including the divergence points of heat capacity. To achieve this, we analyzed four thermodynamic metrics Weinhold (Fig. 6), Ruppeiner (Fig. 7), Quevedo (Fig. 8), and HPEM (Fig. 9) to identify which metric accurately reflects the divergence and zero points of heat capacity in charged black holes within the framework of dilaton-dRGT-like massive gravity. Our findings indicated that the HPEM metric consistently corresponds with all divergence and zero points of heat capacity of charged black holes within the framework of dilaton-dRGT-like massive gravity.

The influence of Maxwell-dilaton-dRGT-like massive black hole parameters on the photonic radius and shadow of the black hole has been explored in the section IV, t. The results highlight that the parameters of the dilaton field, massive gravity, and the graviton mass can measurably affect the photonic orbit. The analysis demonstrates that black hole shadows exhibit rich and distinct behaviors under variations of  $\alpha$ ,  $\eta_1$ ,  $q$ , and  $m_g$ .

In section V, the EHT shadow of  $SgrA^*$  constrains the admissible range of the dilaton coupling and reveals how electromagnetic and massive-gravity effects jointly shape the observable geometry. The derived limits offer a quantitative reference for testing this extended gravity framework against future shadow observations.

In the section VI, our analysis of the energy emission rate reveals that the variations in the dilaton field  $\alpha$ , charge  $q$ , and massive gravity parameters  $\eta_1$  and  $m_g$  distinctly influence both the intensity and spectral distribution of the energy emission. The enhancement of the emission peak with increasing  $\alpha$ ,  $q$ , and  $\eta_1$ , and its suppression by larger  $m_g$ , collectively illustrate how the interplay among scalar, electromagnetic, and massive gravity sectors governs the radiative features of the black hole. Although these results are obtained for specific parameter choices, they consistently demonstrate the characteristic behavior of the Maxwell-dilaton-dRGT-like massive gravity model and provide a useful reference for interpreting possible observational or numerical extensions in similar frameworks.

Black holes are never isolated; they engage with their surroundings and influence the background environment. Following these interactions, black holes emit gravitational waves characterized by quasinormal modes with distinct frequencies. These modes have a non-vanishing imaginary component and encapsulate all information regarding the relaxation of black holes after a perturbation. It is crucial to recognize that quasinormal frequencies are determined by both the geometry of the black hole and the nature of the perturbation applied to the background whether scalar, vector, tensor, or fermionic, and they remain independent of initial conditions. During the ring-down phase of a black hole merger, a uniquely perturbed object emerges, resulting in damped oscillations in the geometry of spacetime due to the emission of gravitational waves. In this context, quasinormal modes (QNMs) are vital for understanding the underlying physics of gravitational waves, with black hole perturbation theory being essential for

this comprehension. Several references, such as [159–162], provide valuable insights into this field, while more recent studies exploring various methods and backgrounds can be found in [163–174] and related references. Gravitational wave astronomy serves as a powerful tool for testing gravity under extreme conditions. Although the literature on the subject is extensive, comprehensive reviews can be found in [175–177]. The study of QNMs is significant not only for constraining black hole parameters but also for its implications for area quantization. Therefore, further investigation into the QN spectrum of black holes in dilaton-dRGT-like-massive gravity is warranted for future research.

The investigation of particle dynamics in the immediate vicinity of black holes is fundamentally essential for probing their geometric and physical characteristics. Over the years, extensive research has been dedicated to exploring the trajectories of both massive and massless particles across various parameterized black hole geometries [178–185]. Consequently, exploring particle dynamics in the context of a black hole embedded within dilaton-dRGT-like massive gravity presents a compelling avenue for future investigation, potentially yielding deeper insights into the geometric and physical properties of this specific system.

### Acknowledgments

The authors express gratitude to the esteemed referee for the valuable comments. This research is supported by the research grant of the University of Mazandaran (33/60679).

- 
- [1] A. G. Riess, et al., *Astron. J* **116**, 1009 (1998).
  - [2] S. Perlmutter, et al., *Astrophys. J* **517**, 565 (1999).
  - [3] D. N. Spergel et al., *Astrophys. J. Suppl.* **148**, 175 (2003).
  - [4] P. A. R. Ade et al., *Astron. Astrophys.* **594**, A13 (2016).
  - [5] K. Koyama, G. Niz, and G. Tasinato, *Phys. Rev. Lett.* **107**, 131101 (2011).
  - [6] A. H. Chamseddine, and M. S. Volkov, *Phys. Lett. B* **704**, 652 (2011).
  - [7] G. D’Amico, et al., *Phys. Rev. D* **84**, 124046 (2011).
  - [8] K. Hinterbichler, *Rev. Mod. Phys.* **84**, 671 (2012).
  - [9] Y. Akrami, T. S. Koivisto, and M. Sandstad, *JHEP* **03**, 099 (2013).
  - [10] S. Weinberg, *Phys. Rev. B* **138**, 988 (1965).
  - [11] D. G. Boulware, and S. Deser, *Ann. Phys.* **89**, 193 (1975).
  - [12] M. Fierz, and W. Pauli, *Proc. R. Soc. Lond. A* **173**, 211 (1939).
  - [13] A. I. Vainshtein, *Phys. Lett. B* **39**, 393 (1972).
  - [14] D. G. Boulware, and S. Deser, *Phys. Rev. D* **6**, 3368 (1972).
  - [15] E. A. Bergshoeff, O. Hohm, and P. K. Townsend, *Phys. Rev. Lett.* **102**, 201301 (2009).
  - [16] C. de Rham, G. Gabadadze, and A. J. Tolley, *Phys. Rev. Lett.* **106**, 231101 (2011).
  - [17] C. de Rham, *Living Rev. Relativity.* **17**, 7 (2014).
  - [18] T. Q. Do, *Phys. Rev. D* **93**, 104003 (2016).
  - [19] T. Q. Do, *Phys. Rev. D* **94**, 044022 (2016).
  - [20] T. M. Nieuwenhuizen, *Phys. Rev. D* **84**, 024038 (2011).
  - [21] A. Gruzinov, and M. Mirbabayi, *Phys. Rev. D* **84**, 124019 (2011).
  - [22] L. Berezhiani, G. Chkareuli, C. de Rham, G. Gabadadze, and A. J. Tolley, *Phys. Rev. D* **85**, 044024 (2012).
  - [23] M. S. Volkov, *Phys. Rev. D* **85**, 124043 (2012).
  - [24] P. Gratia, W. Hu, and M. Wyman, *Phys. Rev. D* **86**, 061504 (2012).
  - [25] C. -I. Chiang, K. Izumi, and P. Chen, *JCAP* **1212**, 025 (2012).
  - [26] E. Babichev, and A. Fabbri, *Class. Quantum Gravit.* **30**, 152001 (2013).
  - [27] R. Brito, V. Cardoso, and P. Pani, *Phys. Rev. D* **88**, 064006 (2013).
  - [28] H. Kodama, and I. Arraut, *Prog. Theor. Exp. Phys.* **2014**, 023E02 (2014).
  - [29] S. Renaux-Petel, *JCAP* **1403**, 043 (2014).
  - [30] E. Babichev, and A. Fabbri, *Phys. Rev. D* **89**, 081502 (2014).
  - [31] S. G. Ghosh, L. Tannukij, and P. Wongjun, *Eur. Phys. J. C* **76**, 1 (2016).
  - [32] B. Eslam Panah, S. H. Hendi, and Y. C. Ong, *Phys. Dark Universe.* **27**, 100452 (2020).
  - [33] P. Chunaksorn, et al., *Eur. Phys. J. C* **82**, 1174 (2022).
  - [34] S. H. Hendi, Kh. Jafarzade, and B. Eslam Panah, *JCAP* **02**, 022 (2023).
  - [35] P. K. Yerra, S. Mukherji, and C. Bhamidipati, *Phys. Rev. D* **111**, 124018 (2025).
  - [36] D. Comelli, M. Crisostomi, F. Nesti, and L. Pilo, *JHEP* **3**, 1 (2012).
  - [37] D. Langlois, and A. Naruko, *Class. Quantum Gravit.* **29**, 202001 (2012).
  - [38] T. Kobayashi, M. Siino, M. Yamaguchi, and D. Yoshida, *Phys. Rev. D* **86**, 061505 (2012).
  - [39] A. De Felice, A. E. Gumrukcuoglu, C. Lin, and S. Mukohyama, *Class. Quantum Gravit.* **30**, 184004 (2013).
  - [40] S. F. Hassan, and R. A. Rosen, *JHEP* **2**, 1 (2012).

- [41] D. Vegh, "Holography without translational symmetry", [arXiv:1301.0537].
- [42] R. -G. Cai, Y. -P. Hu, Q. -Y. Pan, and Y. -L. Zhang, Phys. Rev. D **91**, 024032 (2015).
- [43] S. H. Hendi, B. Eslam Panah, and S. Panahiyan, JHEP **11**, 157 (2015).
- [44] S. H. Hendi, B. Eslam Panah, and S. Panahiyan, Class. Quantum Gravit. **33**, 235007 (2016).
- [45] S. H. Hendi, B. Eslam Panah, and S. Panahiyan, Phys. Lett. B **769**, 191 (2017).
- [46] S. H. Hendi, et al., Eur. Phys. J. C **76**, 571 (2016).
- [47] Y. -B. Ma, R. Zhao, and S. Cao, Commun. Theor. Phys. **69**, 544 (2018).
- [48] Y. Ma, et al., Eur. Phys. J. C **80**, 213 (2020).
- [49] B. Wu, C. Wang, Z. M. Xu, and W. L. Yang, Eur. Phys. J. C **81**, 626 (2021).
- [50] B. Eslam Panah, Kh. Jafarzade, and A. Rincon, Gen. Relativ. Gravit. **56**, 46 (2024).
- [51] P. Paul, S. Upadhyay, and D. V. Singh, Eur. Phys. J. Plus. **138**, 566 (2023).
- [52] D. Chen, Y. He, and J. Tao, Eur. Phys. J. C **83**, 872 (2023).
- [53] A. Ali, and A. Övgün, Eur. Phys. J. C **84**, 378 (2024).
- [54] Kh. Jafarzade, B. Eslam Panah, and M. E. Rodrigues, Class. Quantum Gravit. **41**, 065007 (2024).
- [55] H. Chen, et al., Phys. Dark Universe. **46**, 101617 (2024).
- [56] B. Eslam Panah, Phys. Lett. B **868**, 139711 (2025).
- [57] J. Zhang, and S. -Y. Zhou, Phys. Rev. D **97**, 081501(R) (2018).
- [58] B. P. Abbott et al. (LIGO Scientific and Virgo Collaborations), Phys. Rev. Lett. **116**, 061102 (2016).
- [59] B. P. Abbott et al. (LIGO Scientific and Virgo Collaborations), Phys. Rev. Lett. **116**, 221101 (2016).
- [60] A. S. Goldhaber, and M. M. Nieto, Rev. Mod. Phys. **82**, 939 (2010).
- [61] J. B. Jimenez, F. Piazza, and H. Velten, Phys. Rev. Lett. **116**, 061101 (2016).
- [62] A. F. Ali, and S. Das, Int. J. Mod. Phys. D **25**, 1644001 (2016).
- [63] C. de Rham, J. T. Deskins, A. J. Tolley, and S. -Y. Zhou, Rev. Mod. Phys. **89**, 025004 (2017).
- [64] T. Katsuragawa, S. Nojiri, S. D. Odintsov, and M. Yamazaki, Phys. Rev. D **93**, 124013 (2016).
- [65] S. H. Hendi, G. H. Bordbar, B. Eslam Panah, and S. Panahiyan, JCAP **07**, 004 (2017).
- [66] P. Kareeso, P. Burikham, and T. Harko, Eur. Phys. J. C **78**, 941 (2018).
- [67] M. Yamazaki, T. Katsuragawa, S. D. Odintsov, and S. Nojiri, Phys. Rev. D **100**, 084060 (2019).
- [68] B. Eslam Panah, H. L. Liu, Phys. Rev. D **99**, 104074 (2019).
- [69] A. Bagheri Tudeshti, G. H. Bordbar, and B. Eslam Panah, Phys. Dark Universe. **42**, 101354 (2023).
- [70] J. Sedaghat, et al., Eur. Phys. J. C **84**, 171 (2024).
- [71] B. Eslam Panah, and S. H. Hendi, Europhys. Lett. **125**, 60006 (2019).
- [72] S. H. Hendi, R. B. Mann, S. Panahiyan, and B. Eslam Panah, Phys. Rev. D **95**, 021501(R) (2017).
- [73] T. Koikawa, and M. Yoshimura, Phys. Lett. B **189**, 29 (1987).
- [74] G. W. Gibbons, and K. Maeda, Nucl. Phys. B **298**, 741 (1988).
- [75] D. Brill, and J. Horowitz, Phys. Lett. B **262**, 437 (1991).
- [76] D. Garfinkle, G. T. Horowitz, and A. Strominger, Phys. Rev. D **43**, 3140 (1991).
- [77] R. Gregory, and J. A. Harvey, Phys. Rev. D **47**, 2411 (1993).
- [78] G. T. Horowitz, and A. Strominger, Nucl. Phys. B **360**, 197 (1991).
- [79] S. Mignemi and D. L. Wiltshire, Phys. Rev. D **46**, 1475 (1992).
- [80] S. J. Poletti and D. L. Wiltshire, Phys. Rev. D **50**, 7260 (1994).
- [81] S. J. Poletti, J. Twamley and D. L. Wiltshire, Phys. Rev. D **51**, 5720 (1995).
- [82] K. C. K. Chan, J. H. Horne and R. B. Mann, Nucl. Phys. B **447**, 441 (1995).
- [83] R. G. Cai, J. Y. Ji and K. S. Soh, Phys. Rev. D **57**, 6547 (1998).
- [84] G. Clement, D. Gal'tsov and C. Leygnac, Phys. Rev. D **67**, 024012 (2003).
- [85] A. Sheykhi, M. H. Dehghani, N. Riazi and J. Pakravan, Phys. Rev. D **74**, 084016 (2006).
- [86] S. H. Hendi, J. Math. Phys. **49**, 082501 (2008).
- [87] C. J. Gao and S. N. Zhang, Phys. Rev. D **70**, 124019 (2004).
- [88] C. J. Gao and S. N. Zhang, Phys. Lett. B **605**, 185 (2005).
- [89] A. Sheykhi, M. H. Dehghani and S. H. Hendi, Phys. Rev. D **81**, 084040 (2010).
- [90] S. H. Hendi, A. Sheykhi, M. H. Dehghani, Eur. Phys. J. C **70**, 703 (2010).
- [91] S. H. Hendi, G. H. Bordbar, B. Eslam Panah, and M. Najafi, Astrophys. Space Sci. **358**, 30 (2015).
- [92] P. Fiziev, and K. Marinov, Astrophys. Space Sci. **362**, 8 (2017).
- [93] E. Elizalde, P. Fosalba-Vela, S. Naftulin, and S. D. Odintsov, Phys. Lett. B **352**, 235 (1995).
- [94] S. O. Alexeyev, and M. V. Pomazanov, Phys. Rev. D **55**, 2110 (1997).
- [95] T. Torii, H. Yajima, and K.-i. Maeda, Phys. Rev. D **55**, 739 (1997).
- [96] S. Nojiri, O. Obregon, S. D. Odintsov, and S. Ogushi, Phys. Rev. D **62**, 064017 (2000).
- [97] G. Clement, and D. Gal'tsov, Phys. Rev. D **62**, 124013 (2000).
- [98] S. S. Yazadjiev, Phys. Rev. D **72**, 044006 (2005).
- [99] S. H. Hendi, M. Faizal, B. Eslam Panah and S. Panahiyan, Eur. Phys. J. C **76**, 296 (2016).
- [100] S. H. Hendi, B. Eslam Panah and S. Panahiyan, Prog. Theor. Exp. Phys. **2016**, 103A02 (2016).
- [101] K. A. Moussa, G. Clement, and H. Guennoune, Class. Quantum Gravit. **33**, 065008 (2016).
- [102] F. Moura, Phys. Rev. D **99**, 086008 (2019).
- [103] A. De Felice, A. E. Gumrukcuoglu, and S. Mukohyama, Phys. Rev. Lett. **109**, 171101 (2012).
- [104] A. E. Gumrukcuoglu, C. Lin and S. Mukohyama, JCAP **03**, 006 (2012).

- [105] G. D Amico, G. Gabadadze, L. Hui and D. Pirtskhalava, *Phys. Rev. D* **87**, 064037 (2013).
- [106] A. De Felice, and S. Mukohyama, *Phys. Lett. B* **728**, 622 (2014).
- [107] S. Mukohyama, *JCAP* **12**, 011 (2014).
- [108] S. Kazempour, A. R. Akbarieh, and E. N. Saridakis, *Phys. Rev. D* **106**, 103502 (2022).
- [109] A. E. Gumrukcuoglu, et al., *Phys. Rev. D* **88**, 024023 (2013).
- [110] K. Bamba, et al., *Phys. Rev. D* **89**, 083518 (2014).
- [111] T. Kahniashvili, et al., *Phys. Rev. D* **91**, 041301 (2015).
- [112] D. -J. Wu, and S. -Y. Zhou, *Phys. Lett. B* **757**, 324 (2016).
- [113] S. Anselmi, S. Kumar, D. L. Nacir, and G. D. Starkman, *Phys. Rev. D* **96**, 084001 (2017).
- [114] R. Nakarachinda, and P. Wongjun, *Eur. Phys. J. C* **78**, 827 (2018).
- [115] B. Liu, R. -H. Yue, D. -C. Zou, L. Zhang, Z. -Y. Yang, Q. Pan, *Phys. Rev. D* **109**, 064013 (2024).
- [116] R. -H. Yue, K. -Q. Qian, B. Liu, D. -C. Zou, *Chin. Phys. C* **48**, 075104 (2024).
- [117] D. Kastor, S. Ray, and J. Traschen, *Class. Quantum Gravit.* **26**, 195011 (2009).
- [118] S. H. Hendi, and M. H. Vahidinia, *Phys. Rev. D* **88**, 084045 (2013).
- [119] A. M. Frassino, D. Kubiznak, R. B. Mann, and F. Simovic, *JHEP* **09**, 080 (2014).
- [120] R. A. Hennigar, and R. B. Mann, *Entropy* **17**, 8056 (2015).
- [121] S. -W. Wei, and Y. -X. Liu, *Phys. Rev. D* **91**, 044018 (2015).
- [122] T. Delsate, and R. Mann, *JHEP* **02**, 070 (2015).
- [123] D. Kubiznak, and R. B. Mann, *JHEP* **07**, 033 (2012).
- [124] S. -W. Wei, B. Liang, and Y. -X. Liu, *Phys. Rev. D* **96**, 124018 (2017).
- [125] D. -C. Zou, Y. Liu and R. Yue, *Eur. Phys. J. C* **77**, 365 (2017).
- [126] S. H. Hendi, B. Eslam Panah, S. Panahiyan, and M. Momennia, *Eur. Phys. J. C* **77**, 647 (2017).
- [127] K. Bhattacharya, B. R. Majhi, and S. Samanta, *Phys. Rev. D* **96**, 084037 (2017).
- [128] M. Cadoni, E. Franzin, and M. Tuveri, *Phys. Lett. B* **768**, 393 (2017).
- [129] S. H. Hendi, B. Eslam Panah, and S. Panahiyan, *Fortschr. Phys.* **66**, 1800005 (2018).
- [130] H. -L. Li, and Z. -W. Feng, *Eur. Phys. J. C* **78**, 49 (2018).
- [131] S. H. Hendi, et al., *Chin. Phys. C* **43**, 113106 (2019).
- [132] F. Weinhold, *J. Chem. Phys.* **63**, 2479 (1975).
- [133] F. Weinhold, *J. Chem. Phys.* **65**, 558 (1975).
- [134] G. Ruppeiner, *Phys. Rev. A* **20**, 1608 (1979).
- [135] G. Ruppeiner, *Rev. Mod. Phys.* **67**, 605 (1995).
- [136] H. Quevedo, *J. Math. Phys.* **48**, 013506 (2007).
- [137] H. Quevedo, *Gen. Rel. Grav.* **40**, 971 (2008).
- [138] S. H. Hendi, S. Panahiyan, B. Elam Panah, and M. Momennia, *Eur. Phys. J. C* **75**, 507 (2015).
- [139] S. H. Hendi, S. Panahiyan, and B. Eslam Panah, *Adv. High Energy Phys.* **2015**, 743086 (2015).
- [140] S. H. Hendi, S. Panahiyan, B. Eslam Panah, and Z. Armanfard, *Eur. Phys. J. C* **76**, 396 (2016).
- [141] A. Kazunori, et al., *Astrophys. J. Lett.* **930**, L17 (2022).
- [142] A. Kazunori, et al., *Astrophys. J. Lett.* **875**, L5 (2019).
- [143] V. Perlick, and O. Y. Tsupko, *Phys. Rep.* **947**, 1 (2022).
- [144] V. Perlick, O. Y. Tsupko, and G. S. Bisnovatyi-Kogan, *Phys. Rev. D* **92**, 104031 (2015).
- [145] S. Vagnozzi, et al., *Class. Quantum Gravit.* **40**, 165007 (2023).
- [146] M. Okyay, and A. Övgün, *JCAP* **01**, 009 (2022).
- [147] S. U. Khan, J. Rayimbaev, F. Sarikulov, and O. Abdurakhmonov, *Chin. J. Phys.* **90**, 690 (2024).
- [148] S. U. Khan, and J. Ren, *Chin. J. Phys.* **78**, 141 (2022).
- [149] B. Rahmatov, M. Zahid, S. U. Khan, J. Rayimbaev, I. Ibragimov, Z. Yuldoshev, A. Dauletov, and S. Muminov, *Chin. Phys. C* **49**, 075105 (2025).
- [150] S. U. Khan, J. Rayimbaev, F. Sarikulov, and O. Abdurakhmonov, *Chin. J. Phys.* **90**, 690 (2024).
- [151] S. U. Khan, M. Shahzadi, and J. Ren, *Phys. Dark Univ.* **26**, 100331 (2019).
- [152] S. U. Khan, and J. Ren, *Phys. Dark Univ.* **30**, 100644 (2020).
- [153] T. Do, et al., *Science* **365**, 664 (2019).
- [154] R. Abuter, et al., *Astron. Astrophys.* **636**, L5 (2020).
- [155] K. S. Virbhadra, *Phys. Rev. D* **106**, 064038 (2022).
- [156] S. W. Wei, and Y. X. Liu, *JCAP* **11**, 063 (2013).
- [157] S. H. Hendi, Kh. Jafarzade, and B. Eslam Panah, *JCAP* **2**, 022 (2023).
- [158] Y. Yang, D. Liu, A. Övgün, G. Lambiase, and Z. W. Long, *Phys. Rev. D* **109**, 024002 (2024).
- [159] T. Regge, and J. A. Wheeler, *Phys. Rev.* **108**, 1063 (1957).
- [160] F. J. Zerilli, *Phys. Rev. Lett.* **24**, 737 (1970).
- [161] S. A. Teukolsky, *Phys. Rev. Lett.* **29**, 1114 (1972).
- [162] V. Moncrief, *Phys. Rev. D* **12**, 1526 (1975).
- [163] V. Cardoso, R. Konoplya, and J. P. S. Lemos, *Phys. Rev. D* **68**, 044024 (2003).
- [164] S. Fernando, *Gen. Rel. Grav.* **48**, 24 (2016).
- [165] N. Breton, T. Clark, and S. Fernando, *Int. J. Mod. Phys. D* **26**, 1750112 (2017).
- [166] K. Destounis, G. Panotopoulos, and A. Rincon, *Eur. Phys. J. C* **78**, 139 (2018).
- [167] R. A. Konoplya, A. Zhidenko, and A. F. Zinhailo, *Class. Quant. Grav.* **36**, 155002 (2019).

- [168] A. Rincon, and V. Santos, *Eur. Phys. J. C* **80**, 910 (2020).
- [169] R. C. Pantig, L. Mastrototaro, G. Lambiase, and A. Övgün, *Eur. Phys. J. C* **82**, 1155 (2022).
- [170] S. Fernando, P. A. Gonzalez, and Y. Vasquez, *Eur. Phys. J. C* **82**, 600 (2022).
- [171] L. Balart, S. Belmar-Herrera, G. Panotopoulos, and A. Rincon, *Annals Phys.* **454**, 169329 (2023).
- [172] D. J. Gogoi, A. Övgün, and M. Koussour, *Eur. Phys. J. C* **83**, 700 (2023).
- [173] R. Becar, P. A. Gonzalez, and Y. Vasquez, *Eur. Phys. J. C* **83**, 75 (2023).
- [174] S. Alfaro, et al., *Phys. Rev. D* **109**, 104009 (2024).
- [175] K. D. Kokkotas, and B. G. Schmidt, *Living Rev. Rel.* **2**, 2 (1999).
- [176] E. Berti, V. Cardoso, and A. O. Starinets, *Class. Quant. Grav.* **26**, 163001 (2009).
- [177] R. A. Konoplya, and A. Zhidenko, *Rev. Mod. Phys.* **83**, 793 (2011).
- [178] J. M. Bardeen, W. H. Press, S.A. Teukolsky, *Astrophys. J.* **178**, 347 (1972).
- [179] B. Mashhoon, *Phys. Rev. D* **31**, 290 (1985).
- [180] Z. Stuchlik, J. Schee, *Class. Quantum Gravit.* **27**, 215017 (2010).
- [181] M. Kolos, A. Tursunov, Z. Stuchlik, *Eur. Phys. J. C* **77**, 1 (2017).
- [182] T. Oteev, M. Kolos, Z. Stuchlik, *Eur. Phys. J. C* **78**, 1 (2018).
- [183] S. U. Khan, M. Shahzadi, and J. Ren, *Phys. Dark Univ.* **26**, 100331 (2019).
- [184] M. Zahid, S. U. Khan, and J. Ren, *Chin. J. Phys.* **72**, 575 (2021).
- [185] S. U. Khan, U. Uktamov, J. Rayimbaev, A. Abdujabbarov, I. Ibragimov, and Z. Chen, *Eur. Phys. J. C* **84**, 203 (2024).